Eindhoven University of Technology

MASTER

Runaway electron dynamics in tokamak disruptions

Jakobs, M.A.

Award date:
2010

Link to publication

Disclaimer
This document contains a student thesis (bachelor's or master's), as authored by a student at Eindhoven University of Technology. Student theses are made available in the TU/e repository upon obtaining the required degree. The grade received is not published on the document as presented in the repository. The required complexity or quality of research of student theses may vary by program, and the required minimum study period may vary in duration.

General rights
Copyright and moral rights for the publications made accessible in the public portal are retained by the authors and/or other copyright owners and it is a condition of accessing publications that users recognise and abide by the legal requirements associated with these rights.

- Users may download and print one copy of any publication from the public portal for the purpose of private study or research.
- You may not further distribute the material or use it for any profit-making activity or commercial gain

Take down policy
If you believe that this document breaches copyright please contact us providing details, and we will remove access to the work immediately and investigate your claim.

Download date: 02. Dec. 2024

Runaway electron dynamics in tokamak disruptions

Thesis for the Degree of Master of Science

by

Merlijn Jakobs

Department of Applied Physics

Januari 2010

Abstract

In the light of the current understanding of the adverse effect of CO_2 on the climate of our planet and the expected increase in energy demand over the next decades, is it of great importance that we develop new clean energy sources. Fusion energy promises to be such a source if the formidable physics and technical problems that are associated with it can be overcome.

The most promising reactor concept in fusion research, the tokamak, has one severe drawback. To confine the plasma, i.e. the fuel, it has to maintain a very high current which makes the plasma susceptible to disruptions. Disruptions are events in which the plasma in the reactor is terminated through a sudden loss of plasma energy to the wall resulting in a very fast cooling of the plasma and consequently a large increase in plasma resistivity. The resulting fast decrease in current induces a high electric field in which a part of the electron population can be accelerated to very high energies, the so called runaway electrons. In large tokamaks up to two-thirds of the pre-disruption current can be converted into runaway current, which amounts to about 2 MA in current day devices. These beams of relativistic electrons can do serious damage to the reactor when they are lost from the plasma.

Observations from different tokamak experiments show that there is no runaway electron generation for magnetic fields below 2 Tesla, but a theoretical explanation is still lacking. In this work the dynamics of runaway generation during disruptions are studied with the aim of identifying a mechanism that can explain the experimental results. For this purpose we use a one-dimensional model of runaway electron dynamics, called RUN, that includes the various generation processes and losses and the electric field diffusion self-consistently.

One of the loss mechanisms is the resonant interaction of the runaway electrons with the magnetosonic whistler wave. The growth rate of the wave is inversely proportional to the magnetic field. If the wave is excited, the interaction will increase the pitch angle of the runaway electrons which will result in more synchrotron radiation being emitted. The resulting force will slow the electrons down. It is shown that synchrotron radiation alone cannot reduce the number of runaway electrons sufficiently to explain the 2 Tesla threshold, which was confirmed by the results obtained with RUN.

Runaway electrons can also be lost from the plasma through diffusion induced by magnetic perturbations. Both the case in which the whistler wave induces the perturbations and the effect of a constant perturbation were investigated with RUN. In the case of whistler wave induced perturbations there was inverse relation between the runaway current and the magnetic field strength. The results for a constant magnetic perturbation showed a small proportionality between perturbation strength and runaway current for small perturbations (up to $\delta B/B = 10^{-5}$) and a very strong negative relation for $\delta B/B > 10^{-4}$.

Interaction with whistler waves and losses due to magnetic perturbations are not likely to provide a sufficient explanation for the observed magnetic field dependence of runaway electron generation in tokamaks. The runaway current in the later phases of the discharge is strongly dependent on the number of runaway electrons generated in the early stages of the disruption. Only simulations with a very high density showed negligible numbers of primary runaway

electrons, suggesting that an explanation for the experimental results will have to be found by looking at the influx of impurities during the disruption and the subsequent increase in electron density. The strength of the magnetic field could affect the penetration of impurities towards the plasma center, explaining the observed B-field dependence.

Contents

Chapter 1

Introduction

Since the early days of civilisation the world's demand for energy has been continuously growing, at an ever increasing rate. Given the problems associated with the use of conventional energy sources (pollution, enhanced greenhouse effect, finite resources) and the predicted twofold increase in demand over the next 50 years ([1]), it is clear that new, sustainable sources have to be found.

At the end of the 19th century physicists realised that the stars needed to have an until then unknown source of energy, that was able to provide the huge quantities of energy they radiate. After Einstein published his famous $E = mc^2$ formula, it was clear that this could provide the mechanism behind the energy source of the stars: a tiny amount of mass could yield a huge amount of energy if only there was a mechanism to do this.

It was Francis Aston who discovered in 1919 that four hydrogen atoms weighed slightly more than one helium atom and this inspired Sir Arthur Eddington to speculate about the possibility of fusion as the energy source of stars in a speech to the British Association for the Advancement of Science. In 1939 Hans Bethe published a quantitative calculation that won him the 1968 Nobel prize [2].

Nuclear fusion is a promising candidate to deliver clean, reliable and virtually inexhaustible energy. Relying on the same process that powers the sun and all other stars, scientists and engineers are trying to overcome the challenges associated with using fusion on Earth.

1.1 Fusion

Fusion in general is the merging of two or more particles into one. Since the nuclei of atoms are positively charged, one needs to provide them with enough energy to overcome the Coulomb repulsion that exists between two particles with the same charge. Inside a star, the enormous gravitational pressure provides this energy, but on Earth these pressures are not attainable. Instead, very high temperatures are required.

The exact temperature needed for fusion depends on the particles involved, but for the 'easiest' reaction, between the hydrogen isotopes deuterium and tritium, it is still more than a 100 million Kelvin. At this temperature, matter becomes a *plasma*, a gas in which the atoms have been stripped of one or more

of their electrons. This leaves a mixture of positively charged *ions* and free electrons which is susceptible to electromagnetic fields.

For fusion to be a real energy source, just heating the fuel is not enough. The plasma needs to be confined long enough to allow most of the fuel to undergo fusion and it should be prevented from touching the walls since they would melt at such high temperatures.

There are two approaches to solve this problem: inertial and magnetic confinement. Inertial confinement heats very small pellets of fuel (deuterium/tritium ice) very rapidly, with either laser beams or X-rays, and relies on the inertia of the fuel to keep it together long enough to allow a large fraction of the fuel to react. This method is inherently pulsed, since after each 'shot' the pellet needs to be replaced. During the last years great progress has been made in this field, but this thesis will deal with an aspect of the other line of research: magnetically confined fusion.

Magnetically confined fusion (MCF) uses a magnetic field to confine the plasma, exploiting the fact that charged particles can move along magnetic field lines but not perpendicular to them. There are two main reactor concepts in MCF: the tokamak and the stellarator. The main difference is that in a tokamak the plasma carries a large current to provide the poloidal component of the magnetic field, whereas in a stellarator the complete field is created by external coils.

1.2 Tokamak

The tokamak is the most advanced MCF reactor concept. It is shaped as a torus, with external coils generating a toroidal magnetic field that confines the plasma. Figure 1.1 shows a schematic picture of a tokamak with its different components.

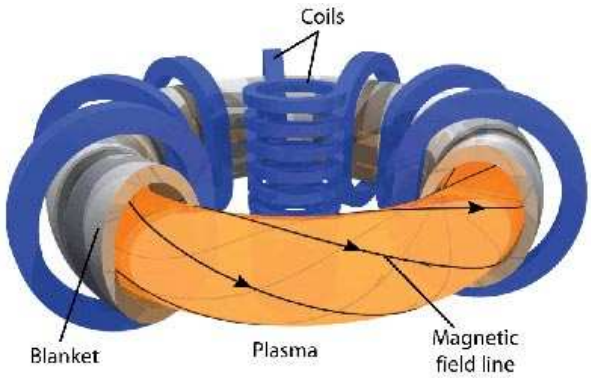

Figure 1.1: A schematic representation of a tokamak with a cutout to reveal plasma and magnetic field lines. Figure courtesy of EFDA.

Charged particles that move in a magnetic field describe helical paths: they are free to move along the field lines, but their motion perpendicular to the field lines is restricted due to the Lorentz force, resulting in a gyrating movement.

The bent field lines in a tokamak cause the particles to drift from the flux surface through two different mechanisms, *gradient B drift* and *curvature drift*.

The first arises from the radial gradient in the magnetic field because of the compression of the field lines on the inside of the torus. During the orbit of a particle the gyration radius varies with the magnetic field strength, resulting in a minimum on the high field side (the inside of the torus) and a maximum on the low field side (outside). This causes the particle to drift slowly in the vertical direction. Because the ions and the electrons gyrate anti-parallel to each other they also have different drift directions, creating a charge separation with the associated electrical field.

The curvature drift on the other hand is not caused by a gradient in field strength, but by the curvature of the field lines. When a particle travels a small distance along a bent field line, it's velocity vector along the field line and the direction of the field line will no longer be aligned. There is component of the field that makes a right angle with the velocity vector of the particle. This component lies in the plane of curvature of the field line, so the drift will be perpendicular to this plane, i.e. in the vertical direction. Since the electrons and the ions have opposite signs of their charge, the Lorentz force will be in different directions. Depending on the direction and magnitude of the plasma rotation, this drift will either enhance or partly cancel the gradient B drift.

This field accelerates and slows down the gyrating particles on the upward and downward part of their orbit (or vice versa, depending on the charge of the particle), resulting in, again, longer or shorter gyration radii and an outward drift of the particle, known as $E \times B$ *drift*. This effect is the same for ions and electrons since the sign of the charge cancels out.

To counteract this effect, the magnetic field is given a poloidal component by running a current in the plasma. The magnetic field lines then follow a helical path around the torus, thus short circuiting the charge separation. The resistance of the plasma scales with $T_e^{3/2}$ (T_e is the electron temperature), so during the beginning of a discharge this provides an easy way to heat the plasma. At high temperatures the resistance of the plasma is very low so only a small toroidal electrical field is required to drive the current.

The worlds largest tokamak, JET, is located in Culham and is currently the holder of the world record for fusion power. In 1997, it produced 16 MW of peak fusion power and 4 MW during steady state[1] operation. The most important parameters of JET are summarised in table 1.1.

Table 1.1: JET main parameters [3]

Major radius	3 m
Minor radius	1.25 m
Magnetic field on axis	4 T
Plasma current	4.3 (7) MA
Current flat top	10 s
Fusion power	16 MW

[1]The power was generated for roughly 5 seconds, which can be regarded as steady state operation from the physics point of view, given the extremely short timescales of most plasma processes.

1.3 Disruptions

A disruption is an unwanted event in a tokamak, during which control over the plasma is lost. The energy present in the plasma in the form of heat, current and fields, is dumped on the wall and this can seriously damage the reactor. A lot of effort is therefore spent on preventing disruptions or, in case of failing prevention, softening them.

The plasma is a highly non-linear medium, which makes it hard to control. Little perturbations of the equilibrium conditions can rapidly grow, in the worst case leading to a complete loss of confinement and a very rapid cooling of the plasma. There are well established experimental limits for operating a tokamak and exceeding these triggers a disruption. Although the causes and accompanying precursors are well known, the precise (microscopic) processes in a disruption remain a topic of further study. For an overview of the development of different disruptions see [4, 5].

The control over the plasma is lost and the resulting transport of plasma energy to the wall causes a large influx of impurities from the wall. The plasma then cools rapidly and consequently the resistance of the plasma increases by several orders of magnitude. This generates a large toroidal electric field, which can accelerate some of the electrons to very high speeds.

1.4 Runaway electrons

When an electron experiences a force from an electric field which is larger than its (time averaged) resistance due to collisions, it will continuously accelerate. Contrary to what one would intuitively expect, the collision frequency of an electron *decreases* with increasing velocity. In a constant electric field this means that once an electron has passed a certain critical velocity, its resistance will drop and the electron will go ever faster. Since the temperature is usually the highest in the centre of the plasma, this is where the probability of runaway electron generation is largest and they tend to be formed in a quite narrow beams (several tens of centimeters across).

In a tokamak there are two possible scenarios in which runaway electrons can be created: during a low density discharge and during a disruption. In the first case a few of the fastest electrons manage to avoid collisions long enough to accelerate past the critical speed. These runaway electrons (or runaways in short) do not really pose a problem since they are relatively few. Furthermore, a reactor will be operated at the higher end of its density range to maximise energy production, so they won't occur in reactor relevant discharges. They might even be put to good use by exploiting them to study magnetic field perturbations [6].

Runaway electrons generated during a disruption are not so benign however and the problem becomes worse with increasing reactor size. The biggest problem is their number and thus the total energy they posses. Because of the large electric fields that arise during a disruption, the critical velocity will be significantly lower than during the steady state phase of the discharge. This means that more electrons will be accelerated past the threshold.

These so called *primary* runaway electrons will at some point collide with another 'normal' electron and can give this electron a strong enough bump to also become a runaway electron. This creates an avalanche which can create

enough runaway electrons to carry roughly two-thirds of the pre-disruption current. In the case of ITER that amounts to around 10 MA which is certain to do great damage to the wall if the electrons hit it.

Experimental observations show that no runaway electrons are generated below a magnetic field of about 2 Tesla [7, 8]. At present it is still unclear what causes this apparent threshold, but a possible explanation might be found in the interaction with whistler waves [9, 10, 11].

1.5 Whistler waves

A magnetised plasma can sustain a variety of electromagnetic waves, *whistler waves* being one of them. Whistler waves also appear in the Earth's atmosphere, where they are excited by lightning. When listening to them by means of a radio receiver they make a whistling sound from which they take their name.

In a tokamak whistler waves can be excited by runaway electrons and may subsequently interact with them, resulting in a change of pitch angle (the angle between the magnetic field lines and the velocity of the electrons) through a scattering process. The growth rate of the wave depends on the magnetic field and might match the observed magnetic field dependence of the occurrence of runaway electrons [11].

1.6 Outline

This thesis will investigate the magnetic field dependence of runaway generation, by studying the runaway electron dynamics in the presence of magnetic field perturbations that may be caused by whistler waves. The structure of the report is as follows.

In Chapter 2 the runaway electron phenomena is introduced by describing the collision operator and the concept of the critical electric field that is needed for runaway generation. The various generation and loss mechanisms and the experimental observation of the magnetic field dependence of the runaway generation are also described.

In Chapter 3 the properties and instability growth rate of the magnetosonic-whistler wave driven by relativistic runaway electrons is given.

Chapter 4 is dedicated to a thorough examination of the runaway electron dynamics in tokamak disruptions. It includes a description of a numerical simulation code that solves the coupled equations of runaway generation and electric field diffusion and its generalisation to include a model of runaway electron losses due to magnetic perturbations and runaway electron and whistler wave interaction. To facilitate comparison with earlier work, we have chosen to use JET shot 63133 as a reference. Therefore all quantitative results presented in this thesis are based on JET parameters.

The Appendices include details of the derivation of the Vlasov equation and the dielectric tensor, and also a description of a more general tool, that can be used for calculating the runaway electron distribution function. In future work this tool could be used for a self-consistent analysis of the runaway dynamics, including a proper model of the velocity-space anisotropy of the runaway distribution.

Chapter 2

Runaway electrons

Runaway electrons take their name from the long mean-free path length and, consequently, the very high velocities they reach in an electrical field. An electron in an electric field experiences an accelerating force. Collisions with other particles in the plasma will slow it down and thus effectively exert a friction force on the electron. However, this friction force *decreases* with increasing energy, resulting in a critical velocity where the drag just balances the acceleration. An electron that manages to avoid collisions long enough to exceed this critical velocity will be accelerated indefinitely and thus 'run away'. In tokamaks, runaway electrons can be created during low density discharges, when the drag due to collisions is low, and more commonly during disruptions as explained in section 1.4. This chapter will deal with the mechanisms behind their generation and ways to detect them. The derivation below follows [12].

2.1 Coulomb collisions

The plasma in a tokamak is completely ionised (if we ignore the odd neutral particle that is created through charge exchange or neutral beam injection), so the particles will 'feel' each others' electrical fields long before they 'touch' each other. In other words: the dominant interactions between particles in a fusion plasma are Coulomb collisions, which occur when two particles pass each other close enough. Close enough in this case means that the distance at which they pas each other, the impact parameter b, is of the order or smaller than λ_D, the Debye length:

$$b \lesssim \lambda_D = \frac{\epsilon_0 T}{ne^2}.$$

This is because the plasma screens out the electric fields of all particles beyond the Debye sphere. As it turns out, for most collisions b is actually of the order of the Debye length, due to the r^3 dependence of the number of particles passing through a sphere with radius r. Most collisions therefore result in only a small deflection. Collisions with $b \ll \lambda_D$ do occur (and head on electron-electron collisions can be important in our case as we will later see), but are far less frequent.

When an electron travels past an ion it will experience an attracting Coulomb force, directed along the line of sight between the particles, which strength is

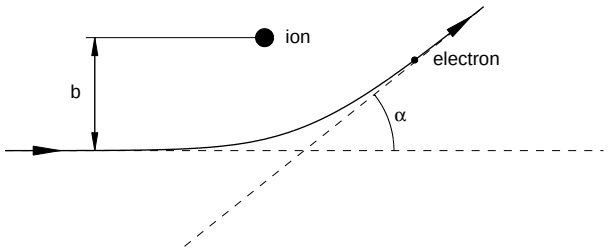

Figure 2.1: A schematic representation of a Coulomb collision between an electron and an ion. The angle α is exaggerated for clarity.

given by

$$F_{\mathrm{C}} = \frac{eq_i}{4\pi\epsilon_0 r^2(t)}, \tag{2.1}$$

where $-e$ and q_i are the charge of the electron and the ion respectively, ϵ_0 is the electric permittivity of free space and $r(t) \simeq (b^2 + v^2t^2)^{1/2}$ is the distance between the two as a function of time. Assuming the electron was originally moving in the x-direction, it will acquire a momentum p_y in the y-direction because of the force exerted on it. The total change in perpendicular momentum is obtained by integrating the component of the force in the y-direction over the whole path of the electron, or in different coordinates, over all time.

$$m_e\Delta v_y = \int_{\infty}^{\infty} \frac{eq_i}{4\pi\epsilon_0 r^2(t)} \frac{b}{r(t)} dt = \frac{eq_i}{4\pi\epsilon_0} \int_{\infty}^{\infty} \frac{bdt}{(b^2 + v^2t^2)^{3/2}} = \frac{eq_i}{4\pi\epsilon_0} \tag{2.2}$$

The bulk of the electrons in a tokamak plasma has a Maxwellian distribution, so $v = v_{Te}$ if the ion is assumed to remain stationary for the duration of the collision. With the assumption that the deflection is small, we find for the angle α

$$\alpha = \frac{\Delta v_y}{v} = \frac{eq_i}{2\pi\epsilon_0 b m_e v_{Te}^2} = \frac{b_{min}}{b}, \tag{2.3}$$

where $b_{min} \equiv eq_i/2\pi\epsilon_0 m_e v_{Te}^2$. Now it is clear the assumption that $\alpha \ll 1$ is valid if $\Lambda \equiv \lambda_D/b_{min} \gg 1$. The so-called *Coulomb logarithm* $\ln\Lambda$ turns out be $\ln\Lambda = 10 - 20$ for a tokamak plasma, which indeed satisfies our criterion.

The effect of all collisions together can be modelled as a friction force:

$$\mathbf{F}_d = m_e \mathbf{v} \nu_{coll}(v), \tag{2.4}$$

where $\nu_{coll}(v)$ is the effective collision frequency for electrons. For thermal electrons, this is dominated by the collisions with ions and collisions with other electrons can be neglected. For (non-relativistic) fast electrons in a tokamak however, also the collisions with bulk electrons contribute to the drag [13] and in this case $\nu_{coll}(v)$ is given by

$$\nu_{coll}(v) = \frac{e^4 n_e \ln\Lambda}{4\pi\epsilon_0^2 m_e^2 v^3}(2 + Z_{eff}). \tag{2.5}$$

2.2 Collision operator

In the previous section the effect of a collision with an ion on the path of an electron was described. But such collisions not only change the direction, but also the speed of the electron. Furthermore, electron-electron collisions occur as well. The exact trajectory of a particle is described by the equations of motion,

$$\dot{\mathbf{r}} = \mathbf{v} \tag{2.6}$$

$$\dot{\mathbf{v}} = \frac{e_a}{m_a}(\mathbf{E} + \mathbf{v} \times \mathbf{B}) \tag{2.7}$$

resulting in 6 coupled equations. It is impossible to solve 6 equations for every particle, but the plasma can be represented with a distribution function $f_a(\mathrm{r}, \mathrm{v}, t)$ for particle species a. The distribution function f_a is defined as the number of particles of species a per unit volume in phase space around the point $\mathbf{z} = (\mathbf{r}, \mathbf{v})$ at time t. Or in other words

$$\int f_a(\mathrm{r}, \mathrm{v}, t) d^3 r d^3 v \tag{2.8}$$

is the number of particles in the volume element around the point $(\mathbf{r}, \mathbf{v})$. The movement in phase space of the particles in a plasma can now be represented as a 'flow', with flow velocity $\dot{\mathbf{z}} = (\dot{\mathbf{r}}, \dot{\mathbf{v}})$.

Since f_a describes a particle density, it also obeys the conservation equation

$$\frac{\partial f_a}{\partial t} + \frac{\partial}{\partial \mathbf{z}}(\dot{\mathbf{z}} f_a) = 0 \tag{2.9}$$

from which the *Vlasov* equation

$$\frac{\partial f_a}{\partial t} + \mathbf{v} \cdot \nabla f_a + \frac{e_a}{m_a}(\mathbf{E} + \mathbf{v} \times \mathbf{B}) \cdot \frac{\partial f_a}{\partial \mathbf{v}} = 0. \tag{2.10}$$

can be derived (see Appendix B). On a small scale the $\mathbf{E}$ and $\mathbf{B}$ fields fluctuate a lot, but for a useful description of the plasma the global fields are much more useful. Since the short range fields only play a role for collisions, their effect can be modelled in a separate collision operator

$$\mathcal{C}_a(f_a) = \left.\frac{\partial f_a}{\partial t}\right|_{collisions},$$

which is moved to the right-hand side of the kinetic equation to form:

$$\frac{\partial f_a}{\partial t} + \mathbf{v} \cdot \nabla f_a + \frac{e_a}{m_a}(\mathbf{E} + \mathbf{v} \times \mathbf{B}) \cdot \frac{\partial f_a}{\partial \mathbf{v}} = \mathcal{C}_a(f_a). \tag{2.11}$$

Here $\mathbf{E}$ and $\mathbf{B}$ are the average fields, which will be the case throughout the remainder of this thesis, unless indicated otherwise.

A plasma always consists of at least two species of particles, so the collision operator for a particle species a is made up of the contributions of collisions with all species b, including $b = a$:

$$\mathcal{C}_a(f_a) = \sum_b \mathcal{C}_{ab}(f_a, f_b) \tag{2.12}$$

The fact that in a plasma most collisions only result in a small change in velocity makes it possible to describe them with a so-called Fokker–Planck collision operator, which takes the form

$$\mathcal{C}_{ab}(f_a, f_b) = \ln\Lambda \left(\frac{q_a q_b}{m_a \epsilon_0}\right)^2 \frac{\partial}{\partial v_k}\left(\frac{m_a}{m_b}\frac{\partial \varphi_b}{\partial v_k} f_a - \frac{\partial^2 \psi_b}{\partial v_k \partial v_l}\frac{\partial f_a}{\partial v_l}\right) \tag{2.13}$$

in tensor notation. In this expression ψ_b and φ_b are the *Rosenbluth* potentials ([14]), defined as

$$\psi_b = -\frac{1}{4\pi}\int \frac{f_b(\mathbf{v}')}{|\mathbf{v}-\mathbf{v}'|} d^3v', \tag{2.14}$$

$$\varphi_b = -\frac{1}{8\pi}\int |\mathbf{v}-\mathbf{v}'| f_b(\mathbf{v}') d^3v'. \tag{2.15}$$

For collisions with a species b that has a Maxwellian distribution function

$$f_b(\mathbf{v}) = f_{Mb}(v) \equiv \frac{n_b}{\pi^{3/2} v_{Tb}^3} e^{-(v/v_{Tb})^2}, \tag{2.16}$$

the Rosenbluth potentials do only depend on the magnitude of $\mathbf{v}$ and not on its direction:

$$\psi_b(\mathbf{v}) = \psi_b(v),$$
$$\varphi_b(\mathbf{v}) = \varphi_b(v).$$

This allows for a reduction of the Fokker–Planck operator to

$$\mathcal{C}_{ab}(f_a, f_b) = \nu_D^{ab}\mathcal{L}(f_a) + \frac{1}{v^2}\frac{\partial}{\partial v}\left[v^3\left(\frac{m_a}{m_a+m_b}\nu_s^{ab} f_a + \frac{1}{2}\nu_\parallel^{ab} v \frac{\partial f_a}{\partial v}\right)\right], \tag{2.17}$$

where $\mathcal{L}$ is the *Lorentz* scattering operator

$$\mathcal{L}(f) \equiv \frac{1}{2}\left[\frac{1}{\sin\theta}\frac{\partial}{\partial\theta}\left(\sin\theta\frac{\partial f}{\partial\theta}\right) + \frac{1}{\sin^2\theta}\frac{\partial^2 f}{\partial\varphi^2}\right]. \tag{2.18}$$

The Lorentz scattering operator describes the diffusion of the direction of the velocity while the magnitude does not change, or, in other words, diffusion on a sphere $v =$ constant in velocity space. The diffusion coefficient is given by the *deflection frequency* ν_D^{ab}. The slowing down frequency of a particle of species a due to collisions with particles of species b is described by ν_s^{ab} in the second term and the last term contains the parallel velocity diffusion frequency $\nu_\parallel^{ab}$.

These three frequencies are most easily described by using the *error* function

$$\mathrm{erf}(x) \equiv \frac{2}{\sqrt{\pi}}\int_0^x e^{-y^2} dy \tag{2.19}$$

and the Chandrasekhar function $G(x)$

$$G(x) \equiv \frac{\mathrm{erf}(x) - x\ \mathrm{erf}'(x)}{2x^2} \to \begin{cases} \frac{2x}{3\sqrt{\pi}}, & x \to 0 \\ \frac{1}{2x^2}, & x \to \infty. \end{cases} \tag{2.20}$$

The frequencies can then be expressed as

$$\nu_D^{ab} \equiv \frac{\langle(\Delta v_\perp/v)^2\rangle^{ab}}{2\Delta t} = \hat{\nu}_{ab}\frac{\mathrm{erf}(x_b) - G(x_b)}{x_a^3}, \tag{2.21}$$

$$\nu_s^{ab} \equiv -\frac{\langle\Delta v_\parallel/v\rangle^{ab}}{\Delta t} = \hat{\nu}_{ab}\frac{2T_a}{T_b}\left(1+\frac{m_b}{m_a}\right)\frac{G(x_b)}{x_a}, \tag{2.22}$$

$$\nu_\parallel^{ab} \equiv \frac{\langle(\Delta v_\parallel/v)^2\rangle^{ab}}{\Delta t} = \hat{\nu}_{ab}\frac{2G(x_b)}{x_a^3}, \tag{2.23}$$

with the basic collision frequency $\hat{\nu}_{ab}$ given by

$$\hat{\nu}_{ab} = \frac{n_b q_a^2 q_b^2 \ln\Lambda}{4\pi\epsilon_0^2 m_a^2 v_{Ta}}. \tag{2.24}$$

In the above equations, x_a and x_b are defined as $x_j = v/v_{Tj}$, the speed of the incoming particle divided by the thermal velocity of particle species j, and $\langle\cdot\rangle$ denotes the statistical average. The subscripts parallel ($_\parallel$) and perpendicular ($_\perp$) refer to the initial direction of the incoming particle.

2.3 Relativistic collision operator

So far relativistic effects have been ignored, since the electron temperature in a tokamak is typically in the 1 – 10 keV range. For a 10 keV electron the relativistic factor γ

$$\gamma = \frac{1}{\sqrt{1-\frac{v^2}{c^2}}} = 1 + p^2$$

is about 1.02, so this is a good approximation. ($p \equiv \gamma v/c$ is the normalised momentum.) However, this is not the case for runaway electrons as they can have energies of several tens of MeV, or $\gamma \sim 40$.

Taking relativistic effects into account, the Fokker–Planck collision operator becomes

$$\mathcal{C}_{ab}(f_a) = \frac{(m_a c)^3}{\hat{\tau}_{ab}}\left[\frac{m_a}{m_b p^2}\frac{\partial}{\partial p}\left(\gamma^2 f_a\right) + \frac{\gamma}{p^3}\mathcal{L}(f_a)\right] \tag{2.25}$$

with $\hat{\tau}_{ab}$ in this case given by

$$\frac{1}{\hat{\tau}_{ab}} = \frac{n_b q_a^2 q_b^2 \ln\Lambda}{4\pi\epsilon_0^2 m_a^2 c^3}. \tag{2.26}$$

2.4 Collision operator valid for both low and high velocities

To be able to model the whole runaway process, a collision operator that is valid both for low velocities (near the critical velocity) and for very high, strongly relativistic velocities is needed. For this purpose a new collision operator has been developed that is constructed such that it is correct both in the low and

high velocity limits. This new collision operator can be used to make more precise calculations of the runaway distribution function.

The collision operator for superthermal electrons ($v \gg v_t$) is given by Karney and Fisch [15] as

$$\mathcal{C}(f) = \frac{1}{p^2}\frac{\partial}{\partial p}p^2\left(A(p)\frac{\partial f}{\partial p} + F(p)f\right) + \frac{2B(p)}{p^2}\mathcal{L}(f), \tag{2.27}$$

with

$$A(p) = \frac{\Gamma v_t^2}{cv^3}, \tag{2.28}$$

$$B(p) = \frac{\Gamma}{2cv}\left(1 + v_t^2\frac{v^4-1}{v^2}\right), \tag{2.29}$$

$$F(p) = \frac{\Gamma v_t^2}{T_e v^2}, \tag{2.30}$$

and

$$\Gamma = \frac{n_e e^4 \ln\Lambda}{4\pi\epsilon_0^2},$$

with v normalised to c so $\gamma^2 = 1/(1-v^2)$ and $v_t^2 = T_e/mc^2$.

Equation (2.27) should be asymptotically matched to the collision operator valid for arbitrary but non-relativistic electrons given in [12], equations 3-40 with 3.45-48. This means that the operators should be the same in a region where they are both valid. Thus that the collision operator that is valid in both regions should look like the one in equation 2.27, with

$$A(p) = \frac{\Gamma v_t^2}{cv^3}2\left(\frac{v}{v_{Te}}\right)^2 G\left(\frac{v}{v_{Te}}\right), \tag{2.31}$$

$$B(p) = \frac{\Gamma}{2cv}\left(1 + v_t^2\frac{v^4-1}{v^2}\right)\left[\phi\left(\frac{v}{v_{Te}}\right) - G\left(\frac{v}{v_{Te}}\right)\right], \tag{2.32}$$

$$F(p) = \frac{\Gamma v_t^2}{T_e v^2}2\left(\frac{v}{v_{Te}}\right)^2 G\left(\frac{v}{v_{Te}}\right), \tag{2.33}$$

where $v_{Te}^2 = 2c^2 v_t^2$. This collision operator can be useful for a more precise calculation of the runaway distribution function, as can be done for instance with the Monte-Carlo method used in the ARENA code [16], see Appendix A. ARENA is capable of calculating the distribution function of the runaway electrons and the toroidal electric field self-consistently (the rise of the runaway current affects the evolution of the electric field, which started the runaway current in the first place). Currently ARENA is the only code capable of solving the kinetic problem including a self-consistent evolution of the electric field, which is crucial for a correct simulation of the dynamical behaviour of the runaways.

2.5 Critical field

An electron (with mass m_e) moving in an electromagnetic field experiences a force given by

$$\mathbf{F}_{em} = q_e(\mathbf{E} + \mathbf{v}\times\mathbf{B}), \tag{2.34}$$

with $\mathbf{F}_{em}$ the electromagnetic force on the electron, $\mathbf{E}$ and $\mathbf{B}$ the electric and magnetic fields respectively and $\mathbf{v}$ the velocity of the electron. Since we are only interested in the movement parallel to the magnetic field the last term on the right-hand side of equation 2.34 can be neglected and using Newton's third law the classical formula for the acceleration of the electron reads

$$\frac{dv}{dt} = \frac{q_e}{m_e}\mathbf{E}. \tag{2.35}$$

This acceleration is balanced by a friction force due to Coulomb collisions which can be derived from equation 2.22

$$F_{fr} = \frac{m_a\langle\Delta v_\parallel\rangle}{\Delta t} = -m_a v_\parallel \nu_s^{ab} \propto G(x_a) \tag{2.36}$$

and is proportional to $G(x_a)$. This reveals a most remarkable property of the friction force, because the Chandrasekhar function is a monotonically decreasing function for high values of x_a, dropping to zero in the limit of infinite velocity. A relativistic analysis shows that this is actually not the case, but merely an artifact of ignoring relativistic effects, and the friction force has a minimum around the electron rest energy at 511 keV. A qualitative plot of the friction force as a function of energy is given in figure 2.2.

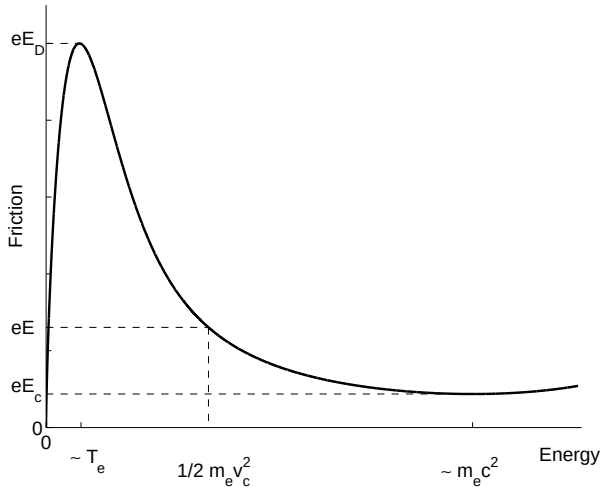

Figure 2.2: The friction force on an electron as a function of temperature.

Equating the electric and the drag force we find the critical velocity

$$v_c = \sqrt{\frac{n_e e^3 \ln\Lambda}{2\pi\epsilon_0^2 m_e E}}, \tag{2.37}$$

or, expressed as critical energy,

$$\frac{m_e v_c^2}{2} = \frac{n_e e^3 \ln\Lambda}{4\pi\epsilon_0^2 E}, \tag{2.38}$$

above which an electron will undergo continuous acceleration. In this expression the contribution from electron-ion collisions has been neglected and it is therefore only valid in the case that $T_e \gg T_i$, so that $\nu_s^{ei} \ll \nu_s^{ee}$.

If one chooses to include electron-ion collisions and the effect of pitch angle scattering (the first term in equation 2.17) in the derivation of the drag force, an extra factor $\sqrt{2 + \mathrm{Z_{eff}}}$ has to be included in the expression for the critical velocity (and consequently any derived quantities).

The so-called *Dreicer* field E_D ([17, 18]) is defined as the field strength for which all electrons, regardless of their initial energy, will run away. Because the friction force has a maximum around the electron thermal velocity, one could say that this is equivalent to $v_c = v_{Te}$:

$$E_D = \frac{n_e e^3 \ln \Lambda}{4\pi\epsilon_0^2 T_e} \tag{2.39}$$

Here T_e is the electron temperature in eV. For runaway generation to occur, it is not necessary that the electric field is as strong as the Dreicer field. The critical field E_c is defined as the field for which the critical energy is equal to the rest energy [19]

$$E_c = \frac{n_e e^3 \ln \Lambda}{4\pi\epsilon_0^2 m_e c^2} \tag{2.40}$$

which is the smallest electrical field for which runaway generation occurs. Usually the electric field in a tokamak does not exceed E_c, but in case of a disruption the induced field might be significantly higher. The critical field also depends on the density, so at low density there can also be runaways during the current plateau phase of the discharge or during the start-up phase of a reactor. Their numbers are usually limited however and they can be used as a tool to study magnetic turbulence [6].

2.6 Generation

2.6.1 Primary generation

From the previous sections the most obvious mechanism for runaway generation is continuous acceleration by the electric field, also known as Dreicer generation. When an electron reaches v_c through diffusion in velocity space, it will be accelerated by the electric field into the runaway regime. The flux of electrons across the threshold is given by

$$\frac{dn_{\mathrm{run}}^I}{dt} = k n_e \hat{\nu}_{ee} \left(\frac{E_D}{E_\parallel}\right)^{3(1+Z_{\mathrm{eff}})/16} \exp\left(-\frac{E_D}{4E_\parallel} - \sqrt{\frac{(1+Z_{\mathrm{eff}})E_D}{E_\parallel}}\right). \tag{2.41}$$

Here k is factor of order unity and Z_{eff} the effective ion charge. This formula was derived by Dreicer assuming an electron population that was in thermal equilibrium when the electric field was applied. This condition is not necessarily satisfied in tokamak disruptions.

2.6.2 Hot tail generation

During the thermal quench of a disruption the thermal electrons lose their energy through interactions with the impurities that enter the plasma. The suprathermal electrons however, interact only weakly with the impurities and lose their energy mainly through collisions with other electrons. Since both processes occur on the scale of the collision time, the thermal electrons will cool down a lot faster than the suprathermal ones, which creates a long tail on the electron velocity distribution.

If the time scale of the temperature quench is of the same order as, or shorter than, the collision time of the suprathermal electrons, these do not have time to thermalise. Part of the electrons in the tail of the distribution can then find themselves having a velocity vv_c and will run away. This process is known as *hot tail* or *burst* generation and is expected to be an important source of primary runaways during ITER disruptions [20, 21, 22].

While the Dreicer generation depends mostly on the electric field, the burst generation mechanism is extremely sensitive to the cooling rate. In JET burst generation dominates Dreicer generation for cooling timescales $t_0 < 0.3$ ms, and for ITER the cross-over point lies around $t_0 \approx 1$ ms [23].

Calculation of the generation rate requires a kinetic treatment of the suprathermal tail of the distribution function by solving the pitch-angle averaged Fokker-Planck equation

$$\frac{\partial f}{\partial t} = \frac{1}{2v^2}\frac{\partial}{\partial v}v^3\left(\nu_s^{ee} f + \nu_\parallel^{ee}\frac{\partial f}{\partial v}\right) + \frac{1}{v^2}\frac{\partial}{\partial v}\left(\nu^{ez} v^3 f\right), \tag{2.42}$$

where the effect of friction and energy diffusion have been included. Here ν^{ez} is the frequency of collisions between electrons and impurities that result in excitation or ionisation, which is only important for the thermal electrons and can be dropped for the suprathermal tail.

2.6.3 Secondary generation

The primary generation processes described above do not take head-on collisions of a runaway electron with other electrons into account. These kind of collisions might be rather infrequent, but if they do occur there is a high chance that after the collision both electrons will have a velocity that is higher than v_c. Both electrons will then be accelerated by the electric field, until they each collide head-on with another electron. These four electrons will then accelerate and the process repeats itself, doubling the number of runaway electrons every collision time.

This avalanche effect acts as a very effective generation process for runaway electrons. The growth rate is given by

$$\frac{1}{n_r}\frac{dn_r}{dt} = \frac{E_\parallel/E_c - 1}{\hat{\tau}_{ee}\ln\Lambda}\sqrt{\frac{\pi\phi}{3(Z_{eff}+5)}} \times \left(1 - \frac{E_c}{E_\parallel} + \frac{4\pi\left(Z_{eff}+1\right)^2}{3\varphi\left(Z_{eff}+5\right)\left(E_\parallel^2/E_c^2 + 4/\varphi^2 - 1\right)}\right), \tag{2.43}$$

where $\varphi = 1 - 1.46\epsilon^{1/2} + 1.72\epsilon$ and $\epsilon = r/R$ is the inverse aspect ratio.

The avalanche mechanism cannot generate primary runaways, but only increase an already present seed population. The seed population can be provided by Dreicer or hot tail generation, but in ITER other possible sources are tritium decay and Compton scattering of γ-rays emitted by activated wall materials [24].

2.7 Loss mechanisms

Generally speaking, the confinement time of runaway electrons is much longer than that of thermal electrons, often up to several seconds. Still, there are several mechanisms through which runaway electrons can be lost. These mechanisms can be divided into two categories, losses to the thermal population and losses to the wall, both of which will be briefly explained below.

2.7.1 Energy loss

Runaway electrons can lose energy by emitting radiation and through collisions with ions and other electrons. Because of the long mean free path length the latter process is rather inefficient and can be completely neglected for runaway electrons that are generated during the steady-state phase of the discharge. For disruption generated runaways it only plays a role when an electron has already slowed down significantly, which requires very long runaway confinement times. In that case the runaway beam will thermalise through collisions towards the very end of the disruption.

Radiation losses mainly occur because an accelerating charged particle emits bremsstrahlung. The acceleration can be due to the momentum exchange in a collision with another particle (which becomes more effective for slower electrons), or because of the gyration motion in the magnetic field, combined with the helical twist and toroidal bending of the field lines when going around the torus. The contributions of the acceleration due to the electrical field can usually be neglected.

Radiation emitted because of the movement of a thermal (non-relativistic) particle in a magnetic field is known as cyclotron radiation. The spectrum consists of a high peak at the first harmonic and smaller peaks at the higher harmonics. Some broadening of the lines will occur due to inhomogeneity of the magnetic field and imperfect orbits because of collisions. When the speed of the particle increases, relativistic effects have to be taken into account and the radiation is then known as synchrotron radiation. The spectrum changes from a discrete to a continuous spectrum and the power is emitted in a cone along the velocity vector that becomes narrower with increasing speed.

For runaway electrons synchrotron radiation is the most important energy loss mechanism and the radiated power is given by

$$P_{sync} = \frac{2}{3}\frac{r_e m_e^2 c^3}{R^2}\beta^4\gamma^4 \tag{2.44}$$

with $r_e = e^2/4\pi\epsilon_0 m_e c^3 = 2.82 \times 10^{-15}$ meter the classical electron radius, $\beta = v/c$ and R is the curvature radius of the motion of the electron. The amount of radiated power is proportional to the fourth power of the speed of the particle, which means that it effectively puts an upper limit on the energy

that can be obtained by a runaway electron, since the power delivered by the electric field is a linear function of the particle velocity.

2.7.2 Radial diffusion

The number of runaway electrons can also decrease through losses to the wall. This can happen by diffusion across the field lines, because even though the electrons move along the field lines, a collision can make them 'hop' onto another field line. The low collisionality of the runaways makes this process very inefficient however, so we will neglect it in the rest of this discussion.

The orbits of the runaway electrons are also radially displaced from the flux surfaces due to the Shafranov shift. This shift becomes larger with increasing energy and when this displacement becomes too large, the electron orbit will intersect with the wall. This puts a maximum on the energy, given by [13]

$$W_{max}^{shift} = \frac{aecB_t}{q_a}. \tag{2.45}$$

In this case a is the minor radius, B_t is the toroidal magnetic field and q_a is the safety factor at the edge. For JET with $q_a = 3$ this gives an energy limit of 375 MeV, corresponding to an orbit shift of 1.25 meter. Runaway electrons that originate on a flux surface away from the plasma center are of course limited to a lower energy, but this limit is not of any practical concern in our case.

There is another mechanism that can cause particles to escape from the plasma which is due to perturbations in the magnetic field itself. The picture of perfectly nested flux surfaces in a tokamak is not automatically valid, especially not during a disruption. The magnetic configuration of the tokamak is inherently topological unstable: small perturbations to the field might lead to the formation of magnetic structures (so-called *islands*) and stochastic regions. Radial transport within these islands or regions regions is greatly increased, which flattens the temperature and density gradient. In a worst case scenario the whole magnetic field becomes stochastic and a field line from the plasma core can end up somewhere on the wall, creating a direct escape route for plasma particles.

A complete description of this process is extremely computationally expensive, but it can be modelled as a diffusion process [25]

$$\frac{\partial n_r}{\partial t} = \frac{1}{r}\frac{\partial}{\partial r} r D_{\mathrm{RR}} \frac{\partial n_r}{\partial r}, \tag{2.46}$$

with D_{RR} the Rechester-Rosenbluth diffusion coefficient, given by

$$D_{\mathrm{RR}} = \pi q v_{\parallel} R \left(\frac{\delta B}{B}\right)^2. \tag{2.47}$$

This approach does not take into account the large gyro-radius of the runaway electrons which, due to the relativistic mass increase, is of the order of the ion Larmor radius. This makes them less susceptible to small scale perturbations and the Rechester-Rosenbluth coefficient therefore overestimates the radial transport of runaway electrons. A more precise treatment is given by Helander et al. in [26].

Mynick and Strachan showed in [27] that the runaway losses are even further reduced when the runaway orbit shift is considered. Because the runaway orbits no longer coincide with the magnetic field surfaces, the electrons pass through different regions of the magnetic field, resulting in a phase averaging over the perturbation. There are even more subtle influences of the different modes of the perturbations, which will not be treated here.

Concluding we can note that magnetic perturbations in general will reduce the confinement of runaway electrons, but a precise quantification is not possible without a detailed treatment of the electron orbits and the spatio-temporal structure of the perturbations.

2.8 Experimental observations

As mentioned previously, runaways are most commonly observed during disruptions, but a closer study reveals that not all disruptions lead to the generation of runaways. Analysis of many disruptions in JET and JT-60 shows that no appreciable number of runaway electrons is generated below a magnetic field of 2 Tesla [7, 8][1]. An overview of JET shots with and without runaways following a disruption can be seen in figure 2.3. This strongly suggests that there is

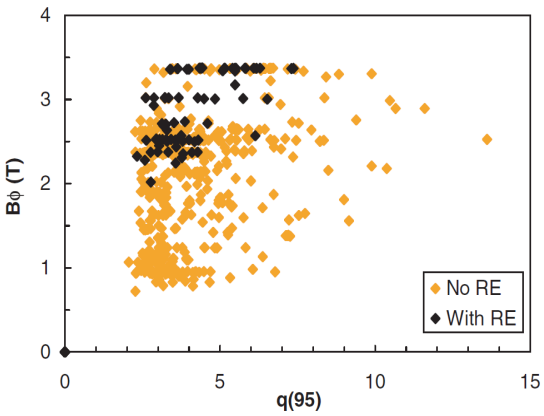

Figure 2.3: Scatter plot of shots with and without runaway electrons after disruptions in JET for different values of the toroidal field B_ϕ and the edge safety factor q_{95}.

some mechanism that inhibits the generation of runaway electrons below about 2 Tesla and one possibility is a a wave-particle interaction, whose onset depends on the magnetic field. Such an interaction exists between relativistic runaway electrons and whistler waves.

The identification of the mechanism behind this correlation between magnetic field strength and the occurence of runaway electrons might show a path towards mitigation of runaway electrons or provide a way of controlling them

[1] Later some runaways were found for magnetic fields below 2 Tesla in the case of massive gas injection in JET [28].

and use them to dissipate the energy stored in the poloidal magnetic field. Given the expected severity of the runaway electron problem in ITER, a complete understanding of their generation and dynamics would be of great advantage.

Chapter 3

Magnetosonic-whistler wave instability

The runaway electron beam has a strongly anisotropic velocity distribution. When the degree of anisotropy exceeds a critical level it can destabilise various plasma waves that have frequencies such that a resonant wave-particle interaction can take place. Previous work has shown that the magnetosonic-whistler waves with frequencies well below the non-relativistic electron cyclotron frequency ω_{ce} but above the ion cyclotron frequency ω_{ci} can be excited by a runaway electron distribution [9, 10]. The wave-particle interaction will lead to very effective pitch-angle scattering and this will increase the amount of synchrotron radiation emitted by the electron. The resulting energy loss will slow the electron down, increasing the number of collisions that it experiences and removing it from the runaway population. In this chapter the properties and instability growth rate of these waves will be discussed.

3.1 Magnetosonic-whistler waves

Non-magnetised plasmas can only support two different kind of waves, high frequency electromagnetic waves and sound like waves. Magnetising the plasma breaks the anisotropy and introduces a preferred direction (the direction of the magnetic field). This allows the propagation of a wide range of waves, one of which is the so-called *whistler* wave.

Whistler waves were discovered when German radio monitors were trying to intercept Allied radio transmissions during World War I [29]. Because of the high dispersion of these waves, they can be heard as a descending tone when using a broad band radio receiver and were therefore named whistlers. Later, it was found out that they are caused by lightning strokes in the southern hemisphere and are guided by the Earth's magnetic field so they could be detected on the northern hemisphere.

Whistler type waves also occur in fusion plasmas, where they take the form of magnetosonic-whistler waves. The magnetosonic wave is a compressional wave that propagates perpendicular to the magnetic field, whereas ordinary whistler waves will follow the field-lines quite closely. The whistler part of the magnetosonic-whistler wave however, is characterised by the large angle between

the magnetic field and the direction of propagation of the wave and should not be confused with magnetospheric whistler waves.

The magnetosonic-whistler waves can be excited by runaway electrons and will subsequently interact with them, resulting in several different phenomena. Since it is really the whistler part of the wave that is responsible for the interaction, this thesis will adopt the convention introduced by [9] and use the term whistler waves.

This chapter will give a brief introduction into wave phenomena in plasmas before analysing the dynamics of the whistler wave in more detail. After that the interaction between the runaway electrons and the wave will be investigated, focusing on the resonances that can destabilise the wave.

3.2 Cold plasma approach

The dynamics of a typical plasma are governed by a wide range of phenomena that make an exact analysis very difficult, not to say impossible. To study the basic properties of the different waves the cold plasma approach is often used. This approach ignores the thermal energy of the electrons and ions, but still all the important wave modes appear.

Other assumptions that need to be made for the derivation below to be valid are that the plasma is homogeneous (both in space and in time) and has no net electric charge, that the magnetic field is homogeneous, that the plasma has an infinite size and that the perturbations are small.

3.3 Homogeneous-plasma wave equation

The equation of motion for a charged particle in an electromagnetic field is given by

$$m\frac{d}{dt}\mathbf{v} = q(\mathbf{E} + \mathbf{v} \times \mathbf{B}) \tag{3.1}$$

with m the mass of the particle, v its speed and q the charge. The electric field $\mathbf{E}$ and magnetic field $\mathbf{B}$ are given by the Maxwell equations

$$\nabla \times \mathbf{E} = -\frac{\partial \mathbf{B}}{\partial t} \tag{3.2}$$

$$\nabla \times \mathbf{B} = \mu_0 \left(\mathbf{J} + \epsilon_0 \frac{\partial \mathbf{E}}{\partial t} \right) \tag{3.3}$$

with μ_0 the magnetic permeability of vacuum and the expression for the total current $\mathbf{J}$

$$\mathbf{J} = \sum_j n_j q_j \mathbf{v}_j \tag{3.4}$$

Here n_j the density of the each species in the plasma and the sum is over all the species.

Applying a Fourier transformation in space and time the homogeneous-plasma wave equation can be derived:

$$\mathbf{k} \times (\mathbf{k} \times \mathbf{E}) + \frac{\omega^2}{c^2} \boldsymbol{\epsilon} \cdot \mathbf{E} = 0 \tag{3.5}$$

with $\mathbf{k}$ the wave-vector, ω the frequency, c the speed of light and $\mathbf{E}(\omega, \mathbf{k})$ the electric field. This is just the ordinary electromagnetic wave equation, with the dielectric constant replaced by the dielectric tensor because of the anisotropy introduced by the magnetic field. The dielectric tensor is defined as

$$\boldsymbol{\epsilon}(\omega, \mathbf{k}) = \mathbf{1} + \sum_j \boldsymbol{\chi}_j(\omega, \mathbf{k}) \tag{3.6}$$

(with $\boldsymbol{\chi}_j$ the susceptibility of species j) and has the benefit that the plasma current $\mathbf{J}$ is expressed in terms of the electric field according to

$$\mathbf{J} - i\omega\epsilon_0\mathbf{E} = i\omega\epsilon_0\boldsymbol{\epsilon} \cdot \mathbf{E} \tag{3.7}$$

This means that the plasma current is treated as a displacement current.

The dielectric tensor has another benefit: it is additive in the contributions from the electrons and the different ion species in the plasma. The contribution from each species is just the species susceptibility $\boldsymbol{\chi}$.

Equation 3.5 is often written as

$$\mathbf{n} \times (\mathbf{n} \times \mathbf{E}) + \boldsymbol{\epsilon} \cdot \mathbf{E} = 0, \tag{3.8}$$

with the introduction of the dimensionless refractive index $\mathbf{n}$

$$\mathbf{n} = \frac{\mathbf{k}c}{\omega}. \tag{3.9}$$

Until now we assumed the plasma particles had no kinetic energy, but this is obviously not a very good description of a fusion plasma. Using a kinetic approach, the finite temperature of the particles can be taken into account. This will result in a modification of the dielectric tensor. For a more complete treatment of waves in thermal, magnetised plasma see [30, 31].

3.4 Dispersion relation for the magnetosonic-whistler wave

Writing out equation 3.5 we obtain the following expression

$$\begin{pmatrix} \frac{\omega^2}{c^2}\epsilon_{11} - k_y^2 - k_z^2 & \frac{\omega^2}{c^2}\epsilon_{12} + k_x k_y & \frac{\omega^2}{c^2}\epsilon_{13} + k_x k_z \\ \frac{\omega^2}{c^2}\epsilon_{21} + k_x k_y & \frac{\omega^2}{c^2}\epsilon_{22} - k_x^2 - k_z^2 & \frac{\omega^2}{c^2}\epsilon_{23} + k_y k_z \\ \frac{\omega^2}{c^2}\epsilon_{31} + k_x k_z & \frac{\omega^2}{c^2}\epsilon_{32} + k_y k_z & \frac{\omega^2}{c^2}\epsilon_{33} - k_x^2 - k_y^2 \end{pmatrix} \begin{pmatrix} E_x \\ E_y \\ E_z \end{pmatrix} = 0 \tag{3.10}$$

If we now choose a rotating coordinate system, so that $\mathbf{B} = (0, 0, B)$ and write $\mathbf{k} = (k_\perp, 0, k_\parallel)$ (where $k_\perp$ and $k_\parallel$ are the components of $\mathbf{k}$ perpendicular and parallel to the magnetic field), equation 3.10 reduces to

$$\begin{pmatrix} \frac{\omega^2}{c^2}\epsilon_{11} - k_\parallel^2 & \frac{\omega^2}{c^2}\epsilon_{12} & \frac{\omega^2}{c^2}\epsilon_{13} + k_\perp k_\parallel \\ \frac{\omega^2}{c^2}\epsilon_{21} & \frac{\omega^2}{c^2}\epsilon_{22} - k^2 & \frac{\omega^2}{c^2}\epsilon_{23} \\ \frac{\omega^2}{c^2}\epsilon_{31} + k_\perp k_\parallel & \frac{\omega^2}{c^2}\epsilon_{32} & \frac{\omega^2}{c^2}\epsilon_{33} - k_\perp^2 \end{pmatrix} \begin{pmatrix} E_x \\ E_y \\ E_\parallel \end{pmatrix} = 0 \tag{3.11}$$

Applying the electromagnetic approximation $E_\parallel = 0$[1], reduces the dimension of this system of equations, so that a non trivial solution to equation 3.5 has to satisfy [32]:

$$\begin{vmatrix} \frac{\omega^2}{c^2}\epsilon_{11} - k_\parallel^2 & \frac{\omega^2}{c^2}\epsilon_{12} \\ \frac{\omega^2}{c^2}\epsilon_{21} & \frac{\omega^2}{c^2}\epsilon_{22} - k^2 \end{vmatrix} = 0 \tag{3.12}$$

Using the fact that the Hall-terms are antisymmetric ($\epsilon_{12} = -\epsilon_{21}$), the characteristic equation 3.12 is given by

$$\left(\epsilon_{11} - \frac{k_\parallel^2 c^2}{\omega^2}\right)\left(\epsilon_{22} - \frac{k^2}{c}^2\ \omega^2\right) + \epsilon_{12}^2 = 0 \tag{3.13}$$

In the case of only one ion species, the dielectric tensor takes the form

$$\boldsymbol{\epsilon}(\omega, \mathbf{k}) = \mathbf{1} + \boldsymbol{\chi}^i(\omega, \mathbf{k}) + \boldsymbol{\chi}^e(\omega, \mathbf{k}) \tag{3.14}$$

where the superscripts i and e denote ions and electrons respectively.

Making some assumptions will greatly simplify this result. For the frequency we assume $\omega_{ci} \ll \omega \ll \omega_{ce}$ (that this is a valid assumption will later be shown when analysing the stability condition for the whistler wave). Other assumptions are $k_\perp^2 v_{Te}^2 \ll \omega^2$ (with v_{Te} the electron thermal velocity), $|\mathbf{k}| \gg |k_\parallel|$ and $\omega_{pi} \ll kc \ll \omega_{pe}$. Applying these to equation 3.13 the magnetosonic-whistler wave dispersion relation

$$\omega = k v_A \sqrt{1 + k_\parallel^2 c^2/\omega_{pi}^2} \tag{3.15}$$

is obtained, where we introduced the Alfvén velocity $v_A = c\omega_{ci}/\omega_{pi}$. For $k_\parallel = 0$ this reduces to the magnetosonic wave $\omega = k v_A$ (pure perpendicular propagation) and for $k_\parallel^2 c^2/\omega_{pi}^2 \gg 1$ to the whistler wave $\omega = k k_\parallel v_A^2/\omega_{ci}$.

3.5 Magnetosonic-whistler wave in the presence of runaway electrons

In the case that runaway electrons are present in the plasma, an extra term has to be added to the dielectric tensor:

$$\boldsymbol{\epsilon}(\omega, \mathbf{k}) = \mathbf{1} + \boldsymbol{\chi}^i(\omega, \mathbf{k}) + \boldsymbol{\chi}^e(\omega, \mathbf{k}) + \boldsymbol{\chi}^r(\omega, \mathbf{k}) \tag{3.16}$$

where $\boldsymbol{\chi}^r$ is the susceptibility of the runaway electrons. Inserting this into equation 3.13 and expanding (see appendix D) gives the dispersion relation

$$\begin{aligned} k^2 v_A^2 \left(1 + \frac{k_\parallel^2 c^2}{\omega_{pi}}\right) - \omega^2 \left(1 + \frac{(k^2 + k_\parallel^2) v_A^2}{\omega_{ci}\omega_{ce}}\right) \\ = \omega^2 \frac{\omega_{ci}^2}{\omega_{pi}^2} \left[\left(1 + \frac{k^2 c^2}{\omega_{pi}}\right)\chi_{11}^r + \left(1 + \frac{k_\parallel^2 c^2}{\omega_{pi}}\right)\chi_{22}^r + 2i\frac{\omega}{\omega_{ci}}\chi_{12}^r\right] \end{aligned} \tag{3.17}$$

[1] So the electric field of the wave is perpendicular to the magnetic background field. This need not be the case for a possible background electric field, for instance during a disruption.

3.6 Magnetosonic-whistler wave instability

In order to calculate the magnetosonic-whistler wave instability growth rate, we need to know the runaway electron distribution function. In previous work the distribution of secondary runaways has been obtained by solving the kinetic equation in the limit when the parallel momentum is much larger than the perpendicular one and using the avalanche growth rate given in (2.43) as a boundary condition [9]. The free energy source driving the instability is the anisotropy in the electron distribution, caused by the acceleration of the runaway electrons in the electric field.

This assumption is valid only in large tokamak disruptions, where the electric field is much larger than the critical field and the interaction with the magnetosonic-whistler waves is neglected during the development of the strongly anisotropic runaway electron velocity distribution. Using the analytical distribution function it has been shown that the growth rates of the most unstable waves are inversely proportional to the magnetic field strength.

The magnetic field depence comes from the contribution from the runaway electrons to the dielectric tensor, χ_{11}^r, which contains an ω_{ce}^2 term that depends on B_t. For typical experimental parameters the whistler branch of the wave is most unstable and therefore in the following we will constrain ourselves to the study of the whistler wave instability.

In order to make a more definite judgement about the importance of the whistler wave instability, it would be necessary to refine the analysis and make a self-consistent simulation of the runaway distribution function and electric field evolution, as could be achieved for instance by the ARENA code [16], could be coupled to an evaluation of the instability growth rate. In that case one solves the kinetic equation numerically, including the interaction with the whistler wave. If the numerical distribution could be obtained as a function of $p_\perp$ and $p_\parallel$ at each time-step, it can be used in a numerical integration scheme to calculate the growth rate of the instability. This would however require a parallelization of ARENA, and is therefore outside the scope of the present thesis. Here we only outline how the numerically obtained distribution could be used for calculation of the whistler wave growth rate.

Taking the growth rate of the whistler wave instability from [9]:

$$\frac{\gamma_i}{\omega_0} = -\frac{k^2 v_A^2}{2\omega_{pi}^2}\mathrm{Im}\chi_{11}^r = \frac{\pi^2\omega_{pr}^2}{\omega_{pi}^2}\frac{k^2 v_A^2}{\omega_0^2}\frac{\omega_{ce}^2}{k_\perp^2 c^2}\frac{1}{k_\parallel c} \times \int_0^\infty dp_\perp \int_{-\infty}^\infty dp_\parallel \sum_{n=-\infty}^{\infty} n^2 J_n^2(z)\delta(p_\parallel + \frac{(n\Omega-\omega_0)\gamma}{k_\parallel c}) \times \left[\frac{n\omega_{ce}}{\gamma}\frac{\partial f_r}{\partial p_\perp} + \frac{k_\parallel c p_\perp}{\gamma}\frac{\partial f_r}{\partial p_\parallel}\right], \quad (3.18)$$

and using the power series formulation of for Bessel functions of the first kind

$$J_n(z) = \sum_{l=0}^{\infty} \frac{(-1)^l}{2^{2l+|n|}l!(l+|n|)!} z^{2l+|n|}, \quad (3.19)$$

which is valid for $|m| \neq \frac{1}{2}$. Taking only the anomalous Doppler resonance into

account ($n = -1$) and squaring we get

$$J_{-1}^2(z) = \left(\frac{z}{2} - \frac{z^3}{16} + \cdots\right)^2 = \frac{z^2}{4} - \frac{z^4}{16} + \cdots . \tag{3.20}$$

Since $z \ll 1$ we only have to keep the first term and substituting for z yields

$$J_{-1}^2(z) \simeq \left(\frac{k_\perp c p_\perp}{4\omega_{ce}}\right)^2 . \tag{3.21}$$

Inserting equation 3.21 into equation 3.18 and taking all constants outside the integrals results in

$$\frac{\gamma_i}{\omega_0} = \frac{\pi^2\omega_{pr}^2}{4\omega_{pi}^2}\frac{k^2 v_A^2}{\omega_0^2}\frac{1}{k_\parallel c}\int_0^\infty dp_\perp\ p_\perp^2 \int_{-\infty}^{\infty} dp_\parallel \delta(p_\parallel - \frac{(\Omega+\omega_0)\gamma}{k_\parallel c}) \times \left[\frac{k_\parallel c p_\perp}{\gamma}\frac{\partial f_r}{\partial p_\parallel} - \frac{\omega_{ce}}{\gamma}\frac{\partial f_r}{\partial p_\perp}\right]. \tag{3.22}$$

For highly relativistic electrons $\gamma = \sqrt{1+p^2} = \sqrt{1+p_\parallel^2+p_\perp^2} \simeq p_\parallel$, so the resonance condition becomes

$$p_\parallel = \frac{\omega_{ce}}{k_\parallel c - \omega_0} = p_{res}. \tag{3.23}$$

Applying this result to equation 3.22 leaves us with

$$\frac{\gamma_i}{\omega_0} = \frac{\pi^2\omega_{pr}^2}{4\omega_{pi}^2}\frac{k^2 v_A^2}{\omega_0^2}\frac{1}{k_\parallel c}\int_0^\infty dp_\perp\ p_\perp^2 \times \left[k_\parallel c p_\perp \left(\frac{k_\parallel c - \omega_0}{\omega_{ce}}\right)\frac{\partial f_r}{\partial p_\parallel} - (k_\parallel c - \omega_0)\frac{\partial f_r}{\partial p_\perp}\right]_{p_\parallel = p_{res}} . \tag{3.24}$$

To obtain the exact growthrate, this needs to be solved for the electron distribution function, but it can be seen that the growthrate depends on B_t through the ω_{ce} factor in the first term on the right (the parallel momentum integral). In the next chapter we will use a heuristic model for a whistler-wave runaway electron interaction, based on the work presented in [11].

Chapter 4

Runaway electron dynamics

In order to study dynamical phenomena in plasmas, computer simulations are an indispensable tool. In our case we have used a modified version of an existing one-dimensional runaway electron simulation code, that was first written by Fredrik Silfverduk under the name READY and subsequently developed by Håkan Smith (STEADY) [33] and Tamás Fehér (GO) [34].

In order to study the magnetic field dependence, we implemented a simple model for the losses induced by whistler wave-runaway electron interaction. Following the informal naming convention, we have called this new code RUN. This chapter will give a brief description of RUN and the different ways of implementing the loss mechanisms. Subsequently the results obtained with the new code are discussed.

4.1 1D simulation of runaway electron dynamics: RUN

A complete description of the runaway electrons requires solving the kinetic equation 2.11 to which a sink term needs to be added to describe the losses. This procedure is computationally very expensive however and it is therefore useful to construct a simpler and coarser model that still contains the essential physics. The most obvious simplifications arise from the fact that a tokamak has two natural spatial symmetries which reduces the dimensionality of the problem by 2. If one is only interested in studying the general behaviour of the generation process, also the distribution function can be approximated by using a Maxwellian distribution for the thermal electrons and by ignoring the velocity space dynamics of the runaway electrons by only looking at their total density n_r.

The RUN code uses both these simplifications and is a 1-D code that calculates the time evolution of the runaway electron density during a disruption in a tokamak. The plasma is assumed to be toroidally and poloidally symmetric, leaving the radial position as the only spatial variable. The program calculates the runaway generation rate from the first and secondary generation mechanisms and uses a diffusive term to describe the losses. Because the cooling timescale that we used, $t_0 = 0.5$ ms, is comfortably above the 0.3 ms cross over point for typical JET plasmas, burst generation is not taken into account to facilitate the

comparison with earlier work. The code can easily be adapted to include hot tail generation however.

The differential equation for the runaway density then takes the following form:

$$\frac{\partial n_r}{\partial t} = \frac{\partial n_r}{\partial t}^{\textbf{Dreicer}} + \frac{\partial n_r}{\partial t}^{\textbf{avalanche}} + \frac{1}{r}\frac{\partial}{\partial r} r D_{rr} \frac{\partial n_r}{\partial r}. \tag{4.1}$$

Here D_{rr} is the Rechester-Rosenbluth diffusion coefficient from section 2.7.2. The diffusion term can be switched on or off depending on the purpose of the simulation, which has been used to investigate the influence of magnetic perturbation on the runaway electron generation. Losses due to resonant interaction with the whistler wave are implemented in a heuristic way, as described below.

The electrical field in RUN follows from the local induction equation in a cylindrical approximation:

$$\frac{1}{r}\frac{\partial}{\partial t}\left(r\frac{\partial E_\parallel}{\partial r}\right) = \mu_0 \frac{\partial j_\parallel}{\partial t} \tag{4.2}$$

where $j_\parallel = \sigma_\parallel E_\parallel + n_r e c$ is the local current density.

A more convenient way of writing these two equations is to use normalised units:

$$\frac{\partial n}{\partial t'} = F\left(E, t', x\right) + nE, \tag{4.3}$$

$$\frac{1}{\alpha x}\frac{\partial}{\partial x} x \frac{\partial E}{\partial x} = \frac{\partial}{\partial t'}\left(\sigma E + n\right). \tag{4.4}$$

In this case $t' = t/3\sqrt{2/\pi}\hat{\tau}_{ee}\ln\Lambda$, $x = r/a$ with a the plasma minor radius and $n = n_r e c/j_{\parallel 0}$, the runaway current normalised to the initial on-axis current density. The conductivity becomes $\sigma = \sigma_\parallel E_{c0}/j_{\parallel 0}$ with E_{c0} the initial critical field on-axis, $E = E_\parallel/E_{c0}$ and $\alpha = (2\pi)^{3/2} j_{\parallel 0} a^2/(3\ln\Lambda I_A)$. The function $F\left(E, t', x\right)$ describes the primary generation and the nE term on the right hand side of equation 4.3 produces the avalanche.

From the initial conditions the program follows a prescribed temperature profile (except that ohmic heating or cooling is taken into account, so the prescribed temperature profile basically gives the rate of energy loss from the plasma). For each time-step it calculates the electrical field and the runaway generation, updates the relevant parameters and progresses with the next time-step.

4.2 Runaway losses due to interaction with whistler waves

The whistler wave model uses the fact that when the growth rate of the wave becomes positive and the wave is excited, it will interact with the runaway electrons through a pitch angle scattering process. This pitch angle scattering then leads to a quick loss of runaway electrons, either because of magnetic perturbations that result in a loss of confinement for the runaway electrons or because of increased energy losses due to synchrotron radiation.

As mentioned previously, an exact calculation of the wave-particle interaction would need a numerical distribution function, which could then be used to determine the growth-rate of every mode of the wave at every point along the minor radius. The distribution function can be obtained with a complete kinetic simulation, as is done by the ARENA code but since this code still needs further development and testing, we decided to do a proof of principle with the RUN code, which is a generalisation of the GO code including the whistler-wave interaction.

The GO code is a 1-dimensional code, that has mainly been used to study the effect of pellet injection on runaway generation. It does not use a physically correct distribution function but assumes that all runaway electrons travel with the speed of light $v = c$ from the moment of their generation. Furthermore, there is no gyration motion, no orbit shift and no magnetic topology. However, the electrical field is calculated self-consistently (including radial diffusion) and one can specify arbitrary radial profiles for density and temperature.

The absence of a distribution function simplifies the problem a lot, at the cost of losing physical correctness. Because it is not possible to calculate the growth-rate of every single mode without distribution function, we took the growth rate of the most unstable mode for an analytic distribution function

$$f(p_\parallel, p_\perp, t) = \frac{C}{p_\parallel} exp\left(\frac{(E-1)t/\tau - p_\parallel}{c_z} - \frac{\alpha p_\perp^2}{2p_\parallel}\right), \tag{4.5}$$

as derived in reference [9]. Here $\alpha = (E-1)/(1+Z)$ and C is given by

$$C = \frac{n_r \alpha}{2\pi c_z} exp\left(-\frac{(E-1)t}{\tau c_z}\right).$$

Then the maximum growth rate can be shown to be

$$\gamma_i^{max} = \frac{\pi}{16}\frac{\omega_{pr}^2}{\omega_{ce}} e^{-1} = 1.3 \times 10^{-9}\frac{n_r}{B_T}, \tag{4.6}$$

where B_T is the local magnetic field in Tesla and the runaway density n_r is the local runaway density.

The total linear growth rate of the wave is determined by the balance between excitation and damping

$$\gamma = \gamma_i^{max} - \gamma_{coll} - \gamma_{conv} \tag{4.7}$$

with the collisional and convective damping terms γ_{coll} and γ_{conv} given by

$$\gamma_{coll} \simeq 1.5\tau_{ei}^{-1}, \tag{4.8}$$

$$\gamma_{conv} \equiv \frac{\partial\omega}{\partial k_\perp}\frac{1}{4L_r} = \frac{v_A^2 k_\parallel}{4\omega_{ci} L_r} \tag{4.9}$$

with $\tau_{ei} = 3\pi^{3/2} m_{e0}^2 v_{Te}^3 \epsilon_0^2 / n_i Z^2 e^4 \ln\Lambda$.

Since we want to investigate whether the observed magnetic field dependence of the runaway generation can be caused by the whister wave interaction, we take a 'worst case' scenario and reduce the number of runaway electrons at the radial position where the wave becomes unstable until the wave is marginally

stable again. In other words: in the simulation the number of runaway electrons is limited by the stability threshold of the wave. This approach was inspired by the fact that the pitch angle scattering happens on a timescale of $t = 3 \times 10^{-7}$ s as was shown in [10], which is four orders of magnitude faster than the runaway electron generation process, which has a timescale of milliseconds.

The way the model is implemented in the numerical calculations means that it is in fact a worse case scenario: we have taken the most unstable mode and used the total number of runaways, not just the ones that are resonant with this mode. Furthermore we have assumed that all runaways above the threshold are instantaneously lost due to synchrotron radiation, which is also an overestimation of the actual losses, as will be shown in the next section.

4.3 Synchrotron radiation

The assumption that the number of runaway electrons is limited by the instability threshold of the wave was inspired by the difference in timescale between the pitch-angle scattering and the runaway generation. However, an electron whose pitch-angle increases is not immediately lost. It still experiences very few collisions and it will still be accelerated by the electrical field. The question is whether the increased energy loss from synchrotron radiation outweighs the energy gain from the electric field.

A gyrating electron in a magnetic field emits radiation, due to the acceleration perpendicular to the field-lines. For thermal electrons this is known as cyclotron radiation, but for relativistic electrons it is called *synchrotron* radiation. The total power emitted by an electron is given by

$$P_{sync} = \frac{2}{3} \frac{r_e m_e^2 c^3}{R^2} \beta^4 \gamma^4 \tag{4.10}$$

with $r_e = e^2/4\pi\epsilon_0 m_e c^3 = 2.82 \times 10^{-15}$ m the classical electron radius, $\beta = v/c$ and R is the curvature radius of the motion of the electron. The path described by a runaway electron is that of a bent helix: the toroidal motion along the field line, the poloidal winding of the field line on its flux surface and the gyration of the electron around the field line. The radius of curvature is then given by

$$R^2 = \frac{\dot{\mathbf{r}}^6}{(\dot{\mathbf{r}} \times \ddot{\mathbf{r}})^2}, \tag{4.11}$$

where $\mathbf{r}$ is the parametrisation function of the bent helix. In most cases the curvature is dominated by the Larmor radius and can then be approximated by

$$\frac{1}{R} = \frac{1 - \xi^2}{R_0} + \frac{eB\xi}{m_e c \gamma} \tag{4.12}$$

with $\xi = p_\perp / p_\parallel$ the pitch-angle of the electron and R_0 the major radius of the tokamak. Figure 4.1 shows the energy gain of a runaway electron moving at the speed of light in JET in a toroidal electric field of 1 Volt per meter as a function of pitch-angle, as well as the radiated power of an electron for different values of γ. For not too large values of the pitch-angle, it is not possible for a runaway electron to lose more energy due to synchrotron radiation than it gains from the electrical field. This is true even for rather low values of the electric field,

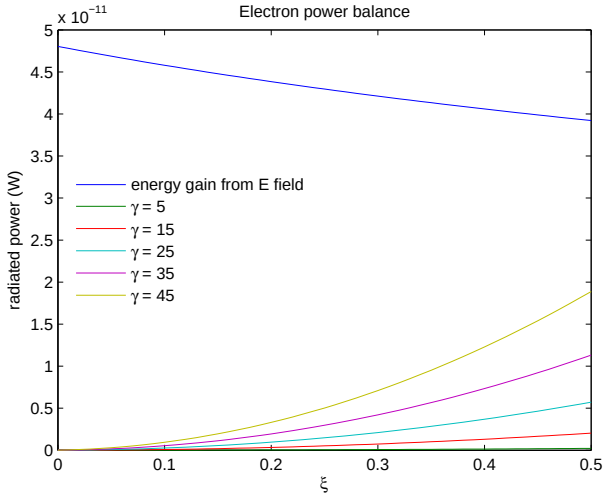

Figure 4.1: The power-loss due to synchrotron radiation of a runaway electron as a function of pitch-angle ξ. The plot is made with JET parameters for a toroidal magnetic field of 3 Tesla and also shows the energy gain per second from an electric field of 1 Vm^{-1}.

as can be seen in figure 4.1. This confirms that the results obtained with the current model give an upper limit to the number of runaway electrons that are lost due to the interaction with whistler waves.

4.4 Magnetic field dependence

The model described above was used to investigate the influence of the whistler wave on the generation of runaway electrons. In particular, we tried to see if we could obtain the same magnetic field dependence as observed on different machines [7, 8], where we have focused on interpreting the JET results. To this end we have taken a typical JET disruption (shot 63133) which main parameters are summarised in Table 4.1.

Table 4.1: Main parameters of JET shot 63133.

Parameter	Value
T_e	3.1 keV
n_e	2.8×10^{19}
B_T	3 T
I_0	1.86 MA
$q_{central}$	1.5

For the temperature a parabolic radial profile was chosen that decays expo-

nentially in time

$$T_e(t,r) = T_{final} + \left[T_0(r) - T_{final}(r)\right]^2 e^{-t/t_0}, \tag{4.13}$$
$$T_0 = (1 - 0.9r^2) \cdot 3.1\text{keV},$$
$$T_{final} = (1 - 0.9r^2)^2 \cdot 10\text{eV},$$

with the temperature quench time $t_0 = 0.5$ ms. It is very hard to obtain good measurements of T_{final} during a disruption, but taking 10 eV as an estimate results in good agreement between experimental observation and runaway models. [35] Given the current understanding of disruptions, the final temperature profile is chosen to be flatter than the initial one. A similar, but static, profile was used for the density

$$n_e(t,r) = (1 - 0.9r^2)^{2/3} \cdot 2.8 \times 10^{19}\text{m}^{-3}. \tag{4.14}$$

The above profiles are the same as the ones used in reference [33] and are based on the experimental data from JET shot 63133. Complete ionisation of the plasma is assumed for the duration of the simulation.

In figure 4.2 the results of a simulation with RUN with the above parameters are displayed. The top left (TL) plot shows the on axis temperature quench on the left axis, whereas on the right axis the on-axis growth and damping rates of the whistler wave, as well as the resulting total on-axis growth rate of the instability can be seen. The runaway density n_r at different radial positions as a function of time can be seen in the top right (TR) plot. The generation in the centre starts slightly earlier than in the more outward regions of the plasma, but the real difference lies in the generation rate after 3 ms, when the thermal quench is completed.

The two middle plots show the runaway density with the beam radius (defined as the radial position where $n_r = n_{r_{max}}/e$) and the electrical field normalised to the Dreicer field. The vertical axis gives the radial position and the horizontal axis is again time. The peak value of the electric field is reached after about 2 ms, when the current has not had enough time to decay. Since the electrical field reaches the highest values on axis, that is where the primary generation of runaway electrons is most efficient. This results in a peaked runaway profile and a faster decay of the electrical field in the center of the plasma. The secondary generation depends less strongly on the electric field strength.

In the bottom left (BL) graph the initial and final ohmic and runaway current densities can be seen as a function of minor radius. The bottom right (BR) figure shows the total, ohmic and runaway currents on the right vertical axis and the central primary and secondary generation rates for the runaway electrons on the left vertical axis, both as function of time.

There is, as expected, no difference between a simulation with whistler wave interaction and without for $B_T = 3$ T, which agrees with the model that predicts that the wave is stabilised for fields above 2 Tesla. For lower fields the effect becomes visible, as can be seen from figures 4.3 and 4.4. Most notable here is the difference in the TL plots: in figure 4.3 the runaway density hits a limit, which is not the case in figure 4.4 where there is no whistler wave interaction present. The electrical field (middle right) decays slower and also diffuses a bit further outward in the case of whistler wave and the BL plot shows that the final current distribution is no longer peaked, but has a flat top due to the imposed upper limit on the number of runaways.

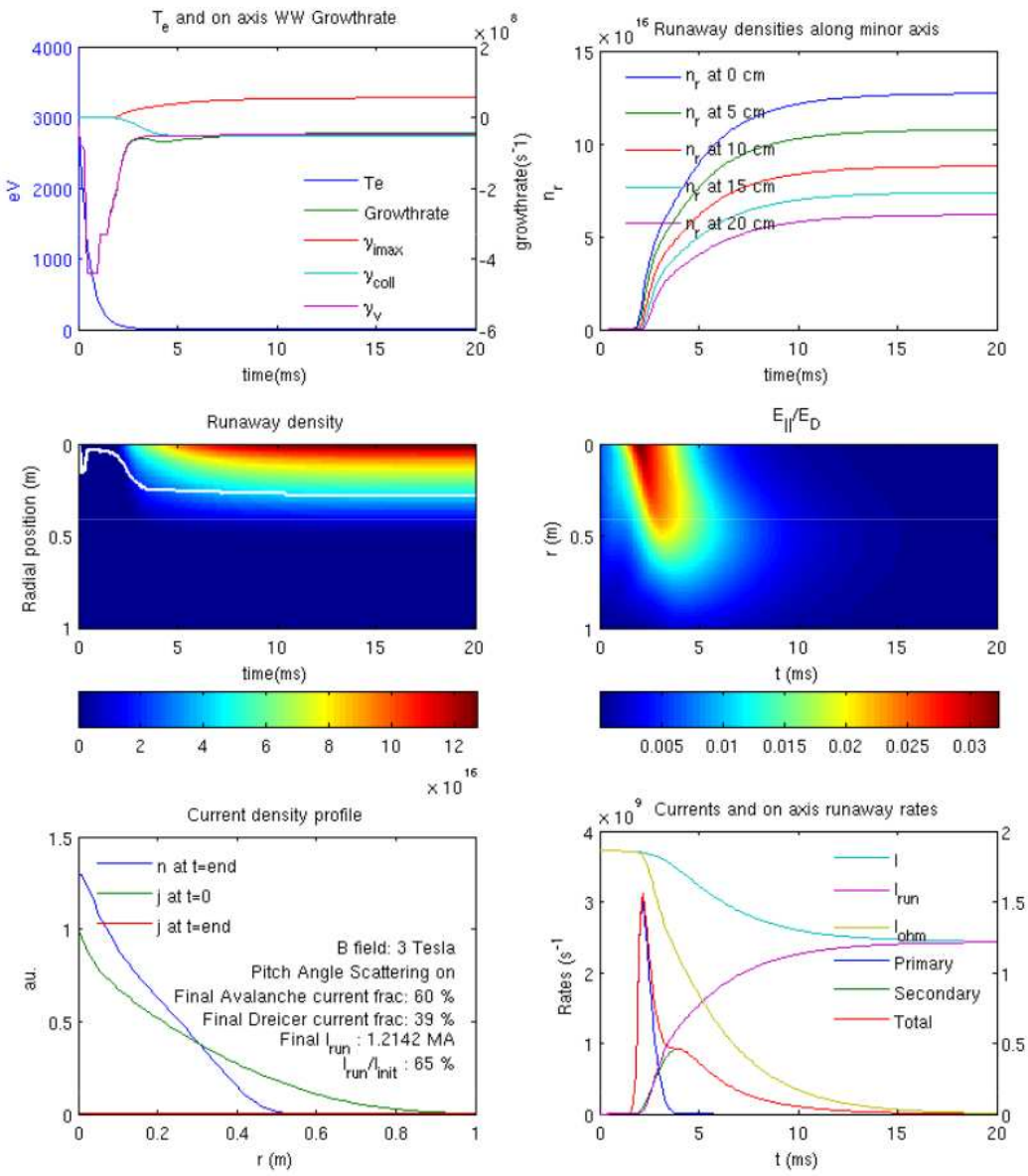

Figure 4.2: A typical result of a RUN simulation of a JET disruption. The meaning of the different plots is explained in the text.

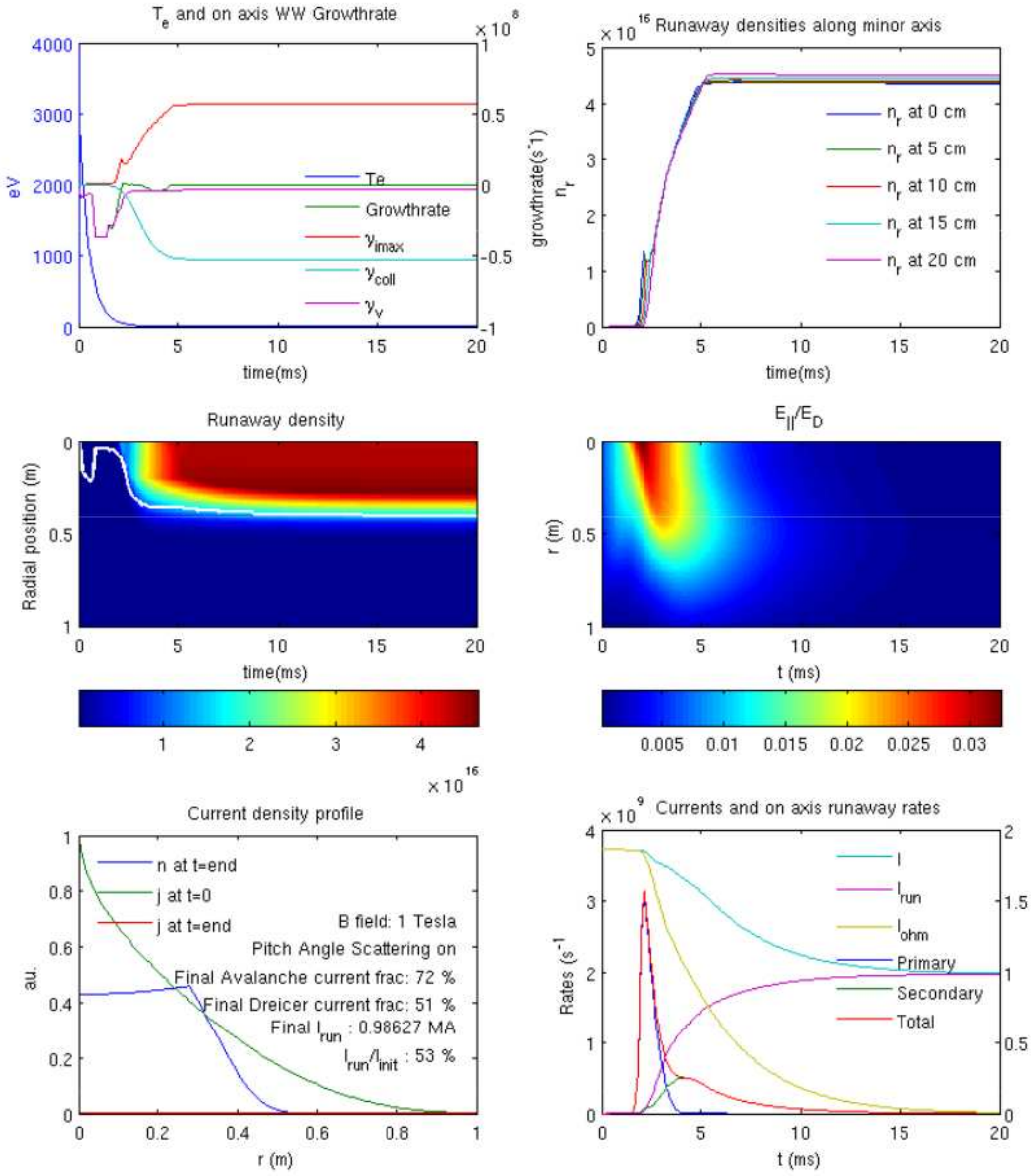

Figure 4.3: Simulation for $B_T = 1$ T with whistler wave interaction.

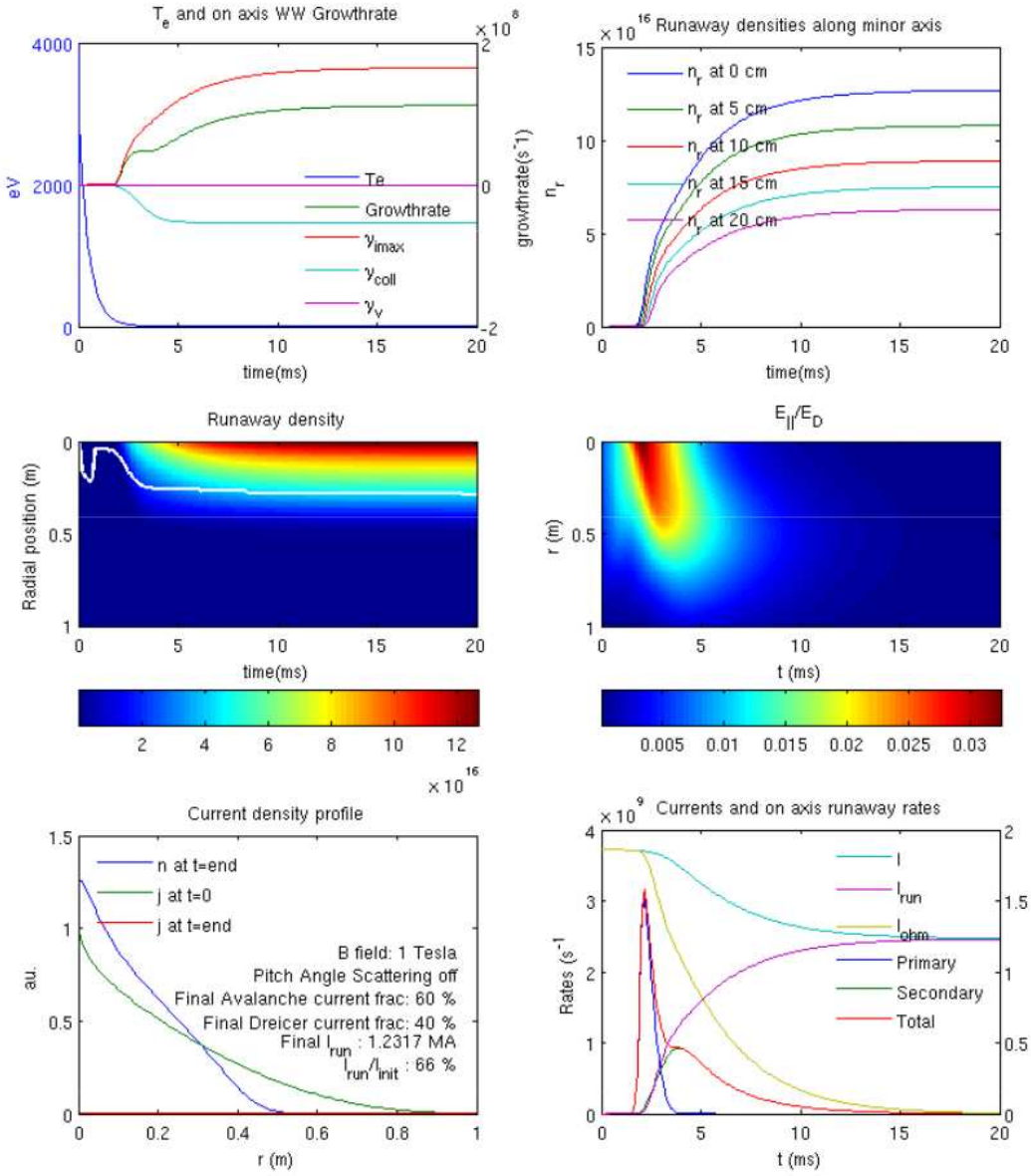

Figure 4.4: Simulation for $B_T = 1$ T without whistler wave interaction.

4.4.1 Whistler wave induced losses

To investigate the influence of the whistler wave a parameter scan was carried out around the parameters of JET shot 63133. The magnetic field was varied between 1 and 4 Tesla and for each toroidal field strength, simulations with 1, 2, 3 and 4 times the original density were run. This was inspired by the fact that the density can increase significantly during a disruption, as has been observed on JET [7].

The parameter of most interest is of course the runaway current I_r, but since the damping of the whistler wave depends on the beam diameter and the beam diameter gives an indication of the current profile, this parameter is also investigated.

Figure 4.5 shows the runaway electron beam diameter as a function of toroidal magnetic field strength for different densities, as well as one magnetic field scan for the standard density. For all densities, the beam diameter decreases for higher field strengths. This is an effect of the outward diffusion of the electrical field that stays high in the center of the plasma because of the limit on the number of runaway electrons due to the whistler wave interaction. The effect of the flattening of the runaway current profile on the beam diameter is minimal due to the steep gradient in n_r.

The influence of the density on the beam is far greater than that of the magnetic field and for higher densities, the magnetic field influence disappears almost completely. The reason for this is that at high densities the generated field is not strong enough to generate a lot of primary runaways and therefore there simply are not enough runaways to excite the wave, so no interaction can take place.

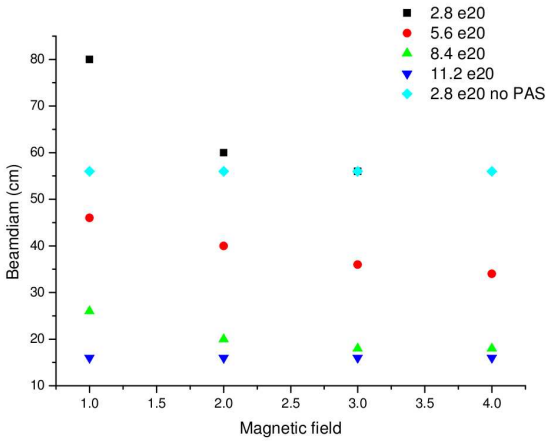

Figure 4.5: The diameter of the runaway electron beam plotted against the toroidal field strength for different densities.

In figure 4.6 the runaway current after 20 milliseconds is plotted as a function of the toroidal magnetic field for different densities. The turquoise points show the final runaway current for simulations without the whistler wave interaction.

The results show a strong dependence of the total number of runaway electrons on density and only for low densities a significant influence on the magnetic field strength is can be seen.

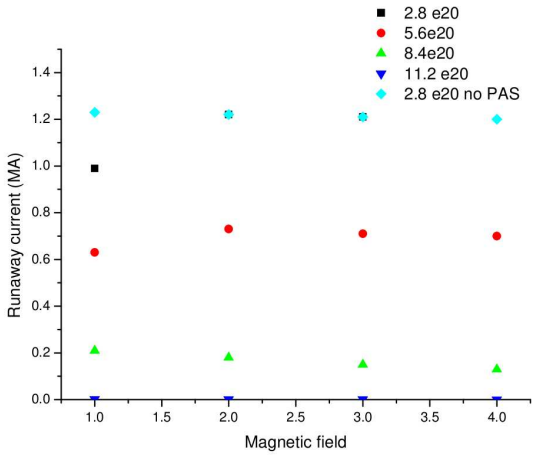

Figure 4.6: The runaway current after 20 ms plotted against the toroidal field strength for different densities.

As explained in 4.2, the implementation of the model gives an upper limit of the losses due to pitch-angle scattering induced synchrotron radiation, suggesting that it is unlikely that the proposed loss mechanism of pitch-angle scattering and consequently increased synchrotron radiation can explain the experimental observations in references [7] and [8].

4.5 Whistler wave induced magnetic perturbations

The model described in the previous subsection was heuristic, since it limited the number of runaways to the marginal instability threshold for the whistler wave without using a physical loss mechanism for the runaway electrons. Also, the results did not agree with the experimental observations of the magnetic field threshold of runaway generation. A possible improvement of the model uses the fact that the whistler wave could create a magnetic perturbation. This perturbation then causes a diffusion of the runaway electrons, providing a physical loss mechanism as described in section 2.7.2.

Since the perturbation is assumed to be induced by the whistler wave, it is introduced at the time when the growth rate of the whistler wave becomes positive. Thus $\delta B = 0$ at start of the simulation and is only changed when $\gamma > 0$ somewhere in the plasma. As soon as $\gamma < 0$, the perturbation is removed again. The strength of the perturbation is unknown and is implemented as a free parameter to see if we could get closer agreement with the experimental results.

Unfortunately, it proved to be quite hard to obtain results with this mechanism, due to numerical stability problems which limited our simulations to a fairly restricted parameter space. The results of a typical simulation for a magnetic field of 1 Tesla, a magnetic perturbation $\delta B/B = 0.01$ and a density of $n_e = 5.6 \times 10^{19}$ m^{-3} are shown in figure 4.7. The final runaway current is about

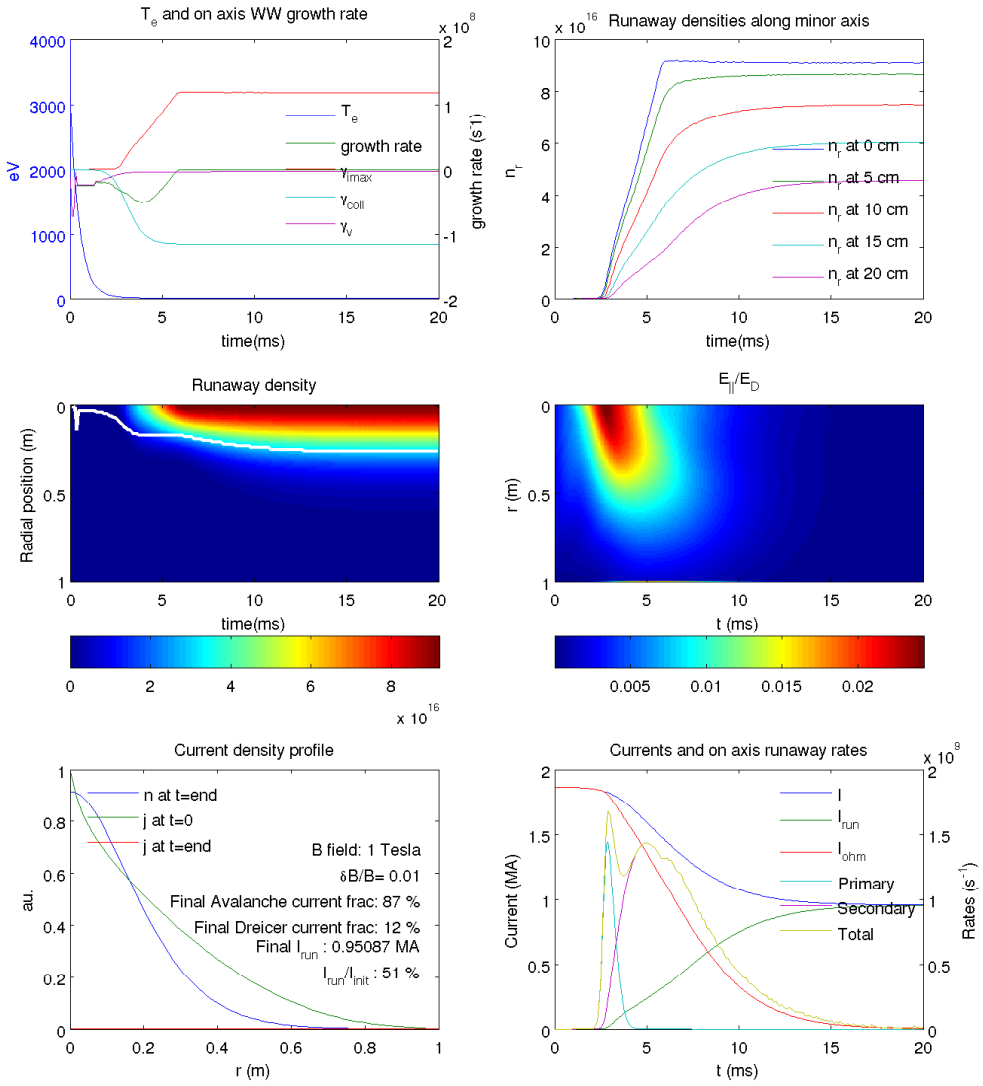

Figure 4.7: The results of a simulation with a $\delta B/B = 0.01$ for a magnetic field of 1 T, where the diffusion only takes place when the whistler wave is excited.

25% higher than the current obtained for the same parameters with $\delta B/B = 0$,

and the beam diameter increases slightly. This is caused by the outward diffusion of the runaway electrons that increase the secondary generation at larger values of r. This effect is a lot stronger than the losses of runaway electrons from the plasma due to diffusion.

All simulations for $\delta B/B < 0.01$ showed the same behaviour: an increase in runaway current and an increase in beam diameter, whereas we could not obtain results for higher perturbation strengths. Nonetheless, we can conclude that the experimental observations cannot be explained by this model.

In figure 4.7 it can be seen that the on-axis runaway density seems to undergo some high frequency fluctuations (the blue line in the top right graph).. This is merely an artifact of the simulation and is the cause of the numerical stability problems that we experienced. If the timescale of diffusion is shorter than the generation timescale, the whistler wave will be constantly at marginal instability. Because of the finite time-steps taken by the program, the number of runaways will decrease to a value that is lower than the threshold value and then increase again until the whistler wave is again excited. To prevent this from happening, the time-step would need to be smaller than the diffusion time scale, which would result in unpractical run-times for the simulations. The problem would be mitigated if perturbation would scale with the strength of the wave. To implement this, a relationship between the amplitude of the wave and the perturbation strength needs to be known, which is currently unavailable.

4.6 Influence of magnetic perturbations

From the previous sections it is clear that the number of primary runaway electrons is not affected by the whistler wave instability. The main reason for this is that the density of runaway electrons required to excite the whistler wave on axis is in the order of $n_{re} = 10^{15}$ m^{-3}, which is only reached at the stage when secondary generation is the dominant mechanism. The avalanche mecanism depends on (primarily generated) seed electrons which are unaffected by the whistler wave instability. To suppress the avalanche mechanism, even higher densities are needed, that can only be achieved with massive gas or pellet injection.

Our first approach did not reduce the number of runaways below the number required for marginal stability of the wave and it appears that this number is high enough that it should have been observed on present day tokamaks. The threshold is equivalent to a runaway current in the order of 0.1 to 1 MA, which is clearly above the detection limit of 1 kA on JET.

A similar argument holds for the introduction of a magnetic perturbation when the whistler wave starts to grow. Even a fairly large perturbation does not increase runaway transport (and consequently losses) fast enough to reduce the number of runaway significantly. Furthermore, the same argument as before holds, that the number already present at the onset of the instability should be above the detection limit.

We therefore investigated the influence of a magnetic perturbation that was present during the whole simulation, to see if this would have the effect of significantly reducing the runaway current. This means the addition of a diffusion term with diffusion coefficient D_{RR} to the right side of equation 4.3. Again, the strength of the magnetic perturbation is a free parameter and we neglect the

effect of orbit shift and orbit averaging.

Figure 4.8 shows the runaway current 20 ms after the start of the disruption plotted against the magnetic field for different densities, in units of 10^{19} m^{-3}, and $\delta B = 0.0004$ T. The value of this magnetic perturbation is reasonable for a disruptive plasma. The electron density is an unknown parameter but it is reasonable to believe that it grows up to an order of magnitude from its original pre-disruption value.

In neither of the cases has the runaway current saturated at a toroidal field of 4 Tesla, but the trend is clearly visible. There is a strong dependence of the runaway current on the magnetic field for the lower density while the effect seems a little weaker for a density of $5.8 \cdot 10^{19}$ m^{-3}. For the highest density it is hard to tell whether there is an effect at all since there is only a very small runaway current (though with 22 kA at 4 Tesla it is still well above the 1 kA detection limit at JET). Figure 4.9, showing the same plot but with the

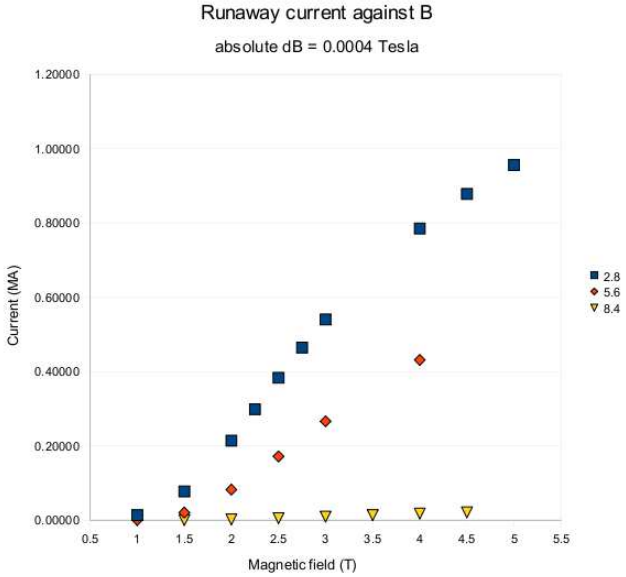

Figure 4.8: The runaway current after 20 ms plotted against the toroidal field strength for different densities (in units of 10^{19} m^{-3}).

current normalised to the runaway current at a magnetic field of 4 Tesla for that density, reveals that the effect actually exists for all three different densities. The curves are shifted a bit to the right for higher densities, indicating that the magnetic field at which the runaway current saturates increases with density. To investigate the influence of the perturbation strength on the runaway current we did a scan of the perturbation strength for a magnetic field of 2 Tesla ata two different densities. The results are shown in figure 4.10, in which the runaway current after 20 ms and the beam diameter are plotted against $\delta B/B$. The final runaway current is not affected up to $\delta B/B$ values of 10^{-6}, from where it starts to increase slightly. Between $\delta B/B = 10^{-5}$ and $\delta B/B = 10^{-4}$, the

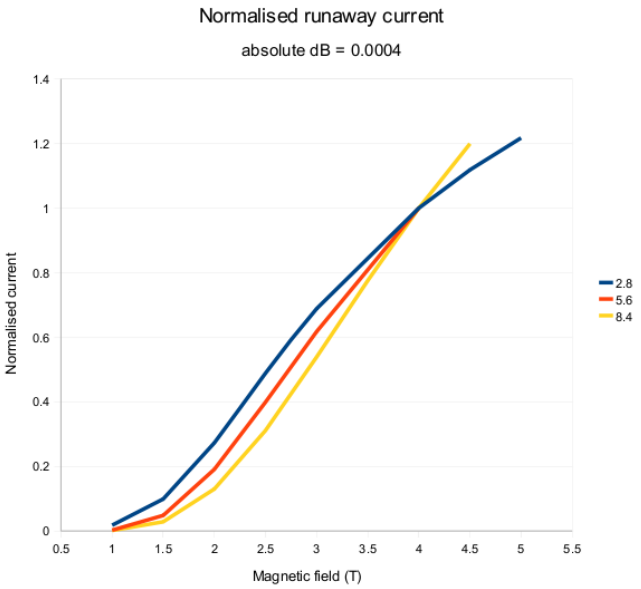

Figure 4.9: The normalised runaway current after 20 ms plotted against the toroidal field strength for different densities (in units of $10^{19}m^{-3}$).

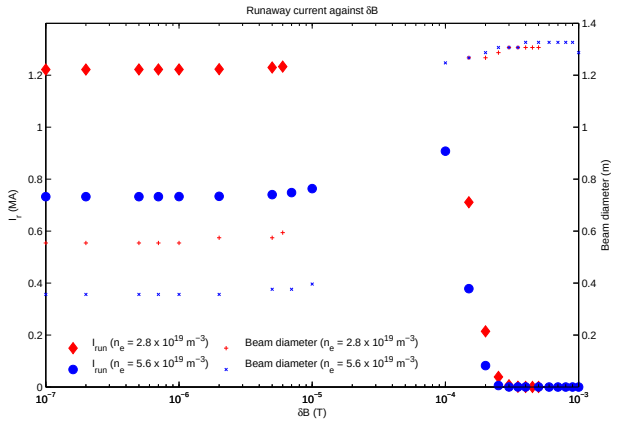

Figure 4.10: The runaway current after 20 ms and the beam diameter plotted against the strength of the magnetic perturbation for a magnetic field of 2 Tesla for two different densities.

simulations cannot be made to converge[1], where the simulations for a density of 2.8×10^{19} m^{-3} are most affected. From $\delta B/B = 10^{-4}$, the final runaway current drops steeply to values of 1 Ampere or less for $\delta B/B > 5 \times 10^{-4}$. The highest point of the $n_e = 5.6 \times 10^{19}$ m^{-3} series is about 25% higher than what the final runaway current is for a simulation without magnetic perturbation.

In the simulations with $\delta B/B < 10^{-5}$, the diffusion has a timescale that is (much) longer than the timescale of secondary runaway generation, which is in agreement with the very long confinement time observed for runaway electrons on present day tokamaks. Therefore, the runaway current reaches a saturation value before it decays away as a result of diffusion and the data from these simulations in figure 4.10 are withing 5% of this saturation current.

Since the primary generation does not depend on the concentration of runaway electrons but only on the parallel electric field, the diffusion only has an indirect influence on this through n_r. The diffusion results in a lower number of runaway electrons in the central part of the plasma, so the electric field decreases slower than it would without diffusion. This results in a primary generation phase that lasts for up to two milliseconds longer, proportionally to magnetic perturbation size.

For the simulations with $\delta B/B > 5 \times 10^{-4}$, this is not the case. Here the time scale of diffusion is comparable to or shorter than the time scale of the secondary generation and hence the runaway current does not reach a saturation value within 20 ms. For these simulations the runaway current reaches a maximum and then decreases. The delay between the primary generation peak and the maximum in the runaway current varies from 9 milliseconds to 0 milliseconds, decreasing with increasing perturbation strength and coinciding with the primary generation peak for $\delta B/B > 10^{-3}$.

The problems for simulations with perturbation strengths $10^{-5} < \delta B/B < 10^{-4}$ were caused by the way the runaway dynamics are implemented in the code. The electric field (equation 4.2) becomes negative if the change in n_r is too big. Again, it is not feasible to just reduce the time-step to shorter values, because of the very long run-time this would require.

Figure 4.10 also shows the beam diameter as a function of δB. The beam diameter increase slightly up to $\delta B/B = 10^{-5}$, and then jumps to 2 to 3 times the original width. It is worth noting that the beam has a different diameter for different densities for low perturbation strengths, whereas for high perturbation amplitudes it is almost the same. This is partly caused by the flattening of the runaway current profile for stronger perturbations and partly by the initial current profile which determines the region where the electrical field will be strong enough to generate runaway electrons. The results suggest that, in the framework of this modelling, it might be possible to use measurement of the runaway beam diameter as a tool to determine the perturbation strength. For application on measurement data, orbit shift, orbit averaging, resonance effects and possibly other mechanisms that can affect the runaway dynamics have to be taken into account.

[1]The problem is that a too large change in n_r causes the electric field to become negative, which is an unphysical solution in this case. The easiest solution would be to shorten the timestep, but the problem is that the runtimes of the simulations quickly approach weeks.

Chapter 5

Conclusions and outlook

From the previous sections we can conclude that our model cannot explain the observations made on modern day tokamaks. The whistler wave interaction requires runaway densities that are easily detectable and also does not sufficiently reduce the number of runaways in the later stages of the disruption.

It would be interesting to compare this tentative conlusion with experimental observations. Since the whistler wave experiences strong convective damping that scales with the beam diameter, it seems unlikely that there will be a strong magnetic signal at the plasma edge. However, the isotropisation effect on the pitch angle could possibly be observed using infrared camera systems as installed on TEXTOR and JET. Extremely fast loss of the runaway electrons ($t_{loss} < 100\mu s$ have already been reported [13], but without complementary data it is not possible to attribute these to whistler waves. Another candidate would be measurement of the beam diameter: since the whistler wave would locally limit the number of runaway electrons, the electric field will diffuse further outward, resulting in a wider beam.

It would also be possible to try and excite the whistler wave during the current flat top of the discharge, by inducing runaway generation through low density and subsequently lowering the toroidal field. Excitation of the wave should be visible in the synchrotron radiation and possibly the x-ray and neutron detectors (depending on whether the loss mechanism is diffusive or radiative or both).

Although the results obtained with our model make it improbable that this mechanism causes the magnetic field dependence, it cannot be completely excluded. Unexpected dynamic effects might change the behaviour of the runaway electrons significantly. Since the RUN code does not contain a distribution function for the runaway electrons, it is not possible to model the wave-particle interaction in more detail. This would require a code that provides a numerical distribution function that can then be used to calculate the growth-rate of all wave modes, which would then affect the kinetics and change the distribution function. The latter part of this approach has already been demonstrated by Pokol *et al* in [10].

The ARENA code would be well suited for this task, but a few challenges need to be overcome. At present, the code cannot be run in parallel which makes any serious use of the code highly unpractical because the large computational expenses result in long run-times. Furthermore, the whistler wave instability

needs to be implemented into the code, or an interface with another code that carries out this part of the simulation needs to be created.

Results obtained from simulations with a magnetic perturbation cannot explain the observed magnetic field dependence of the runaway generation either. The maximum runaway current always falls well within the detectable range, even though the current is reduced to almost zero at the end of the simulations.

All results strongly suggest that an explanation for the magnetic field threshold needs to explain why the primary generation is suppressed, which depends strongly on the induced electric field and the density. Since the electric field is mainly determined by the initial current and there are no reports of an observed threshold in current for runaway electron generation, it seems most likely to look for mechanisms that can increase the density far enough. The relevant density is the density in the region with the highest pre-disruption current (in most cases at the plasma center). It has to be noted that there is of course an indirect relation between the electric field and the magnetic field through j_0 and q, since the electric field depends on j_0 and q depends on both j_0 and B_t.

The present understanding of disruptions is that an instability develops and that triggers an influx of impurities into the plasma, which causes a radiative collapse of the plasma temperature. If the mechanism behind the suppression of the runaway generation is indeed an increase in density, the question arises why this density increase always takes place for disruptions with a magnetic field below 2 Tesla and only for certain shots with a magnetic field above 2 Tesla.

Firstly, the fact that runaway generation can, but does not always occur for magnetic fields stronger than 2 Tesla makes it unlikely that this is the only parameter that determines this bifurcation. This would agree with the recent reports of runaway generation for field below 2T, which hints that runaway generation is possible in a certain volume in a multidimensional parameter space [28]. It appears that the B_t dependence of runaway generation does not show a real threshold, but rather a strong correlation between the occurence of runaway electrons and the magnetic field strength. It does not say much about the absence of runaway electrons since there are numerous disruptions below and above 2 Tesla that show no runaway electrons. Unfortunately, it is not possible to conclude anything on this issue within the scope of this thesis and it therefore requires further investigation.

Secondly, as mentioned previously, it is the density in the region of runaway generation that is important. It is conceivable that in certain cases less impurities penetrate into this region than in other cases. A coupling of a runaway code that implements the full kinetics of the generation process with a transport code might be able to shed some light on this.

A possible way to investigate this experimentally would be to compare the tomographic reconstructions of the bolometer signals (or a radial power density plot) from discharges with and without runaway electrons. The synchrotron radiation or x-ray signal could be used to determine the position of the runaway electron beam ([7, 13]) for the disruptions where they are present. Also direct measurements of the local electron density during a disruption would be of great help in studying this problem.

Appendix A

Avalanche of Runaway Electrons Numerical Analysis (ARENA)

In modern day science many problems are described by equations that are too complex be solved analytically, can only be solved in certain special cases or simply take too long to solve. There is therefore an ongoing search for clever ways to find approximate solutions to these problems, often with the help of computers. The Monte–Carlo method was invented during the Manhattan project by N. Metropolis and S. Ulam ([36]) and has since been developed into a very powerful tool that is applied to a wide range of topics. Because of the nature of the problem, it is well suited for the modelling of runaway electrons. This chapter will give a brief introduction to the Monte–Carlo method and its application in the ARENA code. Subsequently the new Fokker–Planck collision operator will be given and its implementation will be discussed.

A.1 Monte–Carlo method

The simplest way to explain the Monte–Carlo method is by means of an example. Say one wanted to know the value of π and remembered the formula for the area A_c of a circle, $A_c = \pi r^2$ with r the radius of the circle. One way to go about it is to draw a square and then draw a circle inside it with the same diameter as the sides of the square, as shown in figure A.1. The surface A_s of the square is then given by $A_s = d^2 = 4r^2$ and the ratio η of the two surface by

$$\eta = \frac{A_c}{A_s} = \frac{\pi r^2}{4r^2} = \frac{\pi}{4}. \tag{A.1}$$

Now imagine randomly drawing points, or scattering grains of sand within the square. The ratio between the number that fall within the circle to the total number within the square, will be approximately η, getting more precise with a greater number of points.

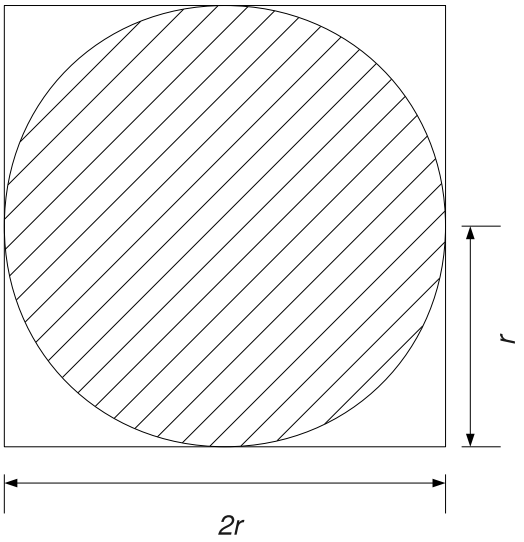

Figure A.1: The ratio between the surface of the circle and the surface of the square is $\pi/4$.

A.1.1 Monte–Carlo theory

If we want to integrate a function f by using the Monte–Carlo method, we calculate the following sum:

$$I_N = \frac{1}{N} \sum_{i=1}^{N} f_i, \tag{A.2}$$

with N the number of sample points. For this to be a valid approximation of the real integral, the following three conditions need to be satisfied.

1. The variables $(f_1, \ldots, f_i, \ldots, f_N)$ have to be statistically independent.
2. The mean value $\mu = \langle f \rangle$ and the variance $\sigma^2 = \langle (f - \langle f \rangle^2) \rangle$
3. N has to be sufficiently large

In that case the expectation value $E[I_N] = \mu = \langle f \rangle$ and the variance is given by

$$\mathrm{Var}[I_N] = \sigma_I^2 = \frac{\sigma_f^2}{N} \tag{A.3}$$

This formula immediately shows the most important drawback of the Monte–Carlo algorithm: it only converges with $\sqrt{N}$. So to double the accuracy, the number of particles needs to be increased fourfold.

Nevertheless, it is the most efficient method for problems of 8 dimensions or higher. Extension to higher dimensions is straightforward: define an input

domain, generate a random sample points within that domain and calculate the result for those points.

When some information is known about the solution this can be used to improve the method. It is possible for instance to use a weighted random distribution function instead of a uniform one to generate the sample points. The distribution function needs to be chosen in such a way that the variance of the result is decreased. One way of doing this is importance sampling, of which the *Metropolis* algorithm is the best known example. It guides the *Markov* chain to the most interesting regions of the sample function, by rejecting a certain fraction of the changes that go in the wrong direction. A Markov chain a stochastic process that exhibits the no–memory property.

A.2 The ARENA program

From the results obtained in chapter 4, it is clear that a simulation code that calculates the distribution function of the runaway electrons would offer great advantages in studying their dynamics during a disruption. One such code is ARENA (Analysis of Runaway Electrons by Numerical Algorithms) which was developed by L.G. Eriksson and P. Helander ([16]).

Simulations of current dynamics during a disruption only need to determine the evolution of the electron distribution function on a time scale that is much longer that the bounce time (the time it takes for a particle to complete one poloidal orbit). This means that the six–dimensional kinetic equation can be reduced to a three–dimensional Fokker–Planck equation by bounce averaging [37]. There are several ways of solving the bounce–averaged Fokker–Planck equation, the most common being finite difference or finite element methods.

However, in the case of runaway electrons there are some particular problems that make these techniques hard to apply. The runaways are continuously accelerated as long a as critical electric field E_c exists [19], which makes it hard to determine the optimal grid size in velocity space. Furthermore, there is a strong radial dependence of the characteristic runaway electron energy. Artifically limiting the energy that the runaway electrons can attain (for instance by introducing very high bremsstrahlung) could mitigate these problems, but would also result in an unphysical distribution function, at least in the high energy region.

Using a Monte–Carlo method to solve the Fokker–Planck equation, which is then replaced by a Langevin equation, such problems do not arise. The Langevin equation describes the trajectory of individual (test) particles, including random effects like collisions, from wich the distribution function can be reconstructed. This elimitates the need for a grid in phase space and puts no limit on the energy a particle can reach. Implementation of this method is fairly simple, making it the approach well suited for runaway electrons.

The main limitiation is the slow convergence as mentioned before ($N^{1/2}$), leading to poor statistics if the number of particles is not high enough. The easiest solution would be to simply increase the number of test particles, but the particles in the thermal part of the distribution are computationally very expensive, due to the high number of collisions they experience. This can be somewhat alliviated by introducing a weighting scheme that increases the weight of the thermal particles and decreases the weight of the test particles in the high

energy part, but for practical applications the code needs to be run in parallel.

A.2.1 Implemenation

The dynamics of the runaway electrons are described by a kinetic equation for the electrons distribution function, that is solved with the Monte–Carlo method, and Maxwells equations for the electric field for which a finite element solver is used. The bounce–averaged Fokker–Planck equation can be written as

$$\frac{\partial f}{\partial t} = \langle L_E(f)\rangle + \langle C(f)\rangle + \langle L_{\text{synch}}(f)\rangle + \langle L_{\text{s.t.}}(f)\rangle + \langle S\rangle + \langle l_B\rangle, \tag{A.4}$$

$$\langle \cdots \rangle = \frac{\oint (\cdots) \frac{d\theta}{2\pi\sqrt{1-\lambda b(\theta)}}}{\oint \frac{d\theta}{2\pi\sqrt{1-\lambda b(\theta)}}}, \tag{A.5}$$

where L_E is the parallel electric field operator, $C(f)$ is the Fokker–Planck collision operator, L_{synch} are the losses due to synchrotron radiation, $L_{\text{s.t.}}$ is an operator representing radial transport, S is a source of secondary-generated runaway electrons and l_B is a loss term of bulk electrons that ensures particle conservation (the integral over phase space of $\langle S + l_B\rangle$ is zero).

The electric field evolution is described by Maxwells equations

$$\nabla \times \mathbf{E} = -\frac{\partial \mathbf{B}}{\partial t}, \tag{A.6}$$

$$\nabla \times \mathbf{B} = \mu_0 \left(\sigma \mathbf{E} + \mathbf{j}_r\right), \tag{A.7}$$

where the displacement current is neglected and the plasma current has been split into the thermal current $\sigma\mathbf{E}$, proportional to σ and carried by f_b the thermal part of the distribution, and $\mathbf{j}_r = -\int e\mathbf{v}\,(f - f_b)\,\mathrm{d}^3\mathrm{v}$, the current carried by the high energy tail of the distribution. The plasma conductivity is aprroximated by

$$\sigma = 1.96\frac{n_e e^2 \tau_e}{m_e}\left(1 - \sqrt{\varepsilon}\right)^2, \tag{A.8}$$

with τ_e the electron collision time and $\varepsilon = r/R$ the inverse aspect ratio. A more complete description of the code can be found in [16].

Appendix B

Derivation of the Vlasov equation

The distribution function f_a gives the number of particles in a volume element d^3rd^3v around the point $(\mathbf{r}, \mathbf{v})$ in phase space. This number can change in two ways: particles can flow into and out of the spatial part of the volume element and they can enter and leave the momentum part through a change in their momentum. The 6D conservation equation

$$\frac{\partial f_a}{\partial t} + \frac{\partial}{\partial \mathbf{z}}(\dot{\mathbf{z}} f_a) = 0 \tag{B.1}$$

can then be written as

$$\frac{\partial f_a}{\partial t} + \frac{\partial}{\partial \mathbf{r}} \cdot (\dot{\mathbf{r}} f_a) + \frac{\partial}{\partial \mathbf{v}} \cdot (\dot{\mathbf{v}} f_a) = 0. \tag{B.2}$$

By using $\frac{\partial}{\partial \mathbf{r}} = \nabla$ and the vector identity $\nabla \cdot f_a \mathbf{v} = f_a \nabla \cdot \mathbf{v} + \mathbf{v} \cdot \nabla f_a$ the second and third terms can be expanded

$$\frac{\partial f_a}{\partial t} + f_a \nabla \cdot \dot{\mathbf{r}} + \dot{\mathbf{r}} \cdot \nabla f_a + f_a \frac{\partial}{\partial \mathbf{v}} \cdot \dot{\mathbf{v}} + \dot{\mathbf{v}} \cdot \frac{\partial f_a}{\partial \mathbf{v}} = 0. \tag{B.3}$$

Now inserting $\dot{\mathbf{r}} = \mathbf{v}$ and $\dot{\mathbf{v}} = e_a/m_a(\mathbf{E} + \mathbf{v} \times \mathbf{B})$ and noticing that

$$\frac{\partial}{\partial \mathbf{v}} \cdot \frac{e_a}{m_a}(\mathbf{E} + \mathbf{v} \times \mathbf{B}) = 0,$$

the conservation equation becomes

$$\frac{\partial f_a}{\partial t} + f_a \nabla \cdot \mathbf{v} + \mathbf{v} \cdot \nabla f_a + \frac{e_a}{m_a}(\mathbf{E} + \mathbf{v} \times \mathbf{B}) \cdot \frac{\partial f_a}{\partial \mathbf{v}} = 0. \tag{B.4}$$

Since $\mathbf{r}$ and $\mathbf{v}$ are independent variables the second term in this expression is zero which gives the Vlasov equation

$$\frac{\partial f_a}{\partial t} + \mathbf{v} \cdot \nabla f_a + \frac{e_a}{m_a}(\mathbf{E} + \mathbf{v} \times \mathbf{B}) \cdot \frac{\partial f_a}{\partial \mathbf{v}} = 0. \tag{B.5}$$

Appendix C

Dielectric tensor

The dielectric tensor for a cold plasma in the notation of [30] is given by

$$\boldsymbol{\epsilon} = \begin{pmatrix} S & -iD & 0 \\ iD & S & 0 \\ 0 & 0 & P \end{pmatrix} \tag{C.1}$$

where the different matrix elements are defined by

$$\begin{aligned} S &= 1 - \sum_a \frac{\omega_{pj}^2}{\omega^2 - \omega_{cj}^2} \\ D &= \sum_a \frac{\omega_{ci}\omega_{pj}^2}{\omega(\omega^2 - \omega_{cj}^2)} \\ P &= 1 - \sum_a \frac{\omega_{pj}^2}{\omega^2} \end{aligned} \tag{C.2}$$

with ω the frequency of the perturbation and ω_{pj} and ω_{cj} the plasma frequency

$$\omega_{pj} = \frac{n_a q_a^2}{m_a \epsilon_0} \tag{C.3}$$

and cyclotron frequency

$$\omega_{cj} = \frac{q_a B_0}{m_a} \tag{C.4}$$

for species a. Note that ω_{cj} has a different sign for ions and electrons, resulting in a different sign for D as well. In our case we only need S and D (see section 3.4) so we will leave out P from here on.

For the magnetosonic whistler wave, the frequencies satisfy $\omega_{ci} \ll \omega \ll \omega_{ce}$. Then equations C.2 reduce to

$$\begin{aligned} S &= 1 - \frac{\omega_{pi}^2}{\omega^2} \\ D &= \frac{\omega_{ci}\omega_{pi}^2}{\omega^3} \end{aligned} \tag{C.5}$$

for the ions and

$$S = 1 + \frac{\omega_{pe}^2}{\omega_{ce}^2}$$
$$D = \frac{\omega_{ce}\omega_{pe}^2}{\omega\omega_{ce}^2} \tag{C.6}$$

for the electrons. We will subsequently drop the one, since all terms are large compared to 1. The runaway contribution to the dielectric tensor can be found in [30, 31].

Appendix D

Derivation of the magnetosonic-whistler wave dispersion relation in the presence of runaway electrons

Starting with equation 3.13 and inserting equation 3.16 we obtain

$$\left(1+\chi_{11}^{i}+\chi_{11}^{e}+\chi_{11}^{r}-\frac{k_{\parallel}^{2}c^{2}}{\omega^{2}}\right)\left(1+\chi_{22}^{i}+\chi_{22}^{e}+\chi_{22}^{r}-\frac{k^{2}c^{2}}{\omega^{2}}\right) + \left(\chi_{12}^{i}+\chi_{12}^{e}+\chi_{12}^{r}\right)^{2}=0 \quad \text{(D.1)}$$

Since for all ion terms in the dielectric tensor $\chi^{i} \gg 1$, we can drop the 1. Expanding the brackets, we get

$$\begin{aligned}\chi_{11}^{i}\chi_{22}^{i}+\chi_{11}^{e}\chi_{22}^{e}+\chi_{11}^{r}\chi_{22}^{r}+\frac{k^{2}k_{\parallel}^{2}c^{4}}{\omega^{4}} \\ +\chi_{11}^{i}\chi_{22}^{e}+\chi_{22}^{i}\chi_{11}^{e}+\chi_{11}^{i}\chi_{22}^{r}+\chi_{22}^{i}\chi_{11}^{r}+\chi_{11}^{e}\chi_{22}^{r}+\chi_{22}^{e}\chi_{11}^{r} \\ -\left(\chi_{11}^{i}+\chi_{11}^{e}+\chi_{11}^{r}\right)\frac{k^{2}c^{2}}{\omega^{2}}-\left(\chi_{22}^{i}+\chi_{22}^{e}+\chi_{22}^{r}\right)\frac{k_{\parallel}^{2}c^{2}}{\omega^{2}} \\ +\left(\chi_{12}^{i}\right)^{2}+\left(\chi_{12}^{e}\right)^{2}+\left(\chi_{12}^{r}\right)^{2} \\ +2\chi_{12}^{i}\chi_{12}^{e}+2\chi_{12}^{i}\chi_{12}^{r}+2\chi_{12}^{e}\chi_{12}^{r}=0 \quad \text{(D.2)}\end{aligned}$$

We now assume that the contribution of the runaway electrons to the dielectric tensor is small compared to the ion and electron terms, so we can throw away all non-linear runaway terms. Using equations C.5 and C.6 with the assumptions from section 3.4: $k_{\perp}^{2}v_{Te}^{2} \ll \omega^{2}$, $|\mathbf{k}| \gg |k_{\parallel}|$ and $\omega_{pi} \ll kc \ll \omega_{pe}$), this takes the

form

$$k^2 v_A^2 \left(1 + \frac{k_\parallel^2 c^2}{\omega_{pi}}\right) - \omega^2 \left(1 + \frac{(k^2 + k_\parallel^2) v_A^2}{\omega_{ci}\omega_{ce}}\right)$$
$$= \omega^2 \frac{\omega_{ci}^2}{\omega_{pi}^2} \left[\left(1 + \frac{k^2 c^2}{\omega_{pi}}\right) \chi_{11}^r + \left(1 + \frac{k_\parallel^2 c^2}{\omega_{pi}}\right) \chi_{22}^r + 2i \frac{\omega}{\omega_{ci}} \chi_{12}^r\right] \quad \text{(D.3)}$$

where the Alfvén velocity is $v_A = c\omega_{ci}/\omega_{pi}$.

Bibliography

[1] J. Ongena and G. V. Oost, "Energy for future centuries," in Uckan [38], pp. 3–15.

[2] H. A. Bethe, "Energy production in stars," *Phys. Rev.*, vol. 55, pp. 434–456, Mar 1939.

[3] EFDA-JET, "JET main features." `http://www.jet.efda.org/wp-content/uploads/JET-main-features.pdf`, 2008.

[4] J. A. Wesson, R. D. Gill, M. Hugon, F. C. Schuller, J. A. Snipes, D. J. Ward, D. V. Bartlett, D. J. Campbell, P. A. Duperrex, A. W. Edwards, R. S. Granetz, N. A. O. Gottardi, T. C. Hender, E. Lazzaro, P. J. Lomas, N. L. Cardozo, K. F. Mast, M. M. F. Nave, N. A. Salmon, P. Smeulders, P. R. Thomas, B. J. D. Tubbing, M. F. Turner, and A. Weller, "Disruptions in jet," *Nuclear Fusion*, vol. 29, pp. 641–666, April 1989.

[5] F. C. Schuller, "Disruptions in tokamaks," *Plasma Physics and Controlled Fusion*, vol. 37, no. 11A, pp. A135–A162, 1995.

[6] I. Entrop, N. J. Lopes Cardozo, R. Jaspers, and K. H. Finken, "Scale size of magnetic turbulence in tokamaks probed with 30-mev electrons," *Phys. Rev. Lett.*, vol. 84, pp. 3606–3609, Apr 2000.

[7] R. Gill, B. Alper, M. de Baar, T. Hender, M. Johnson, V. Riccardo, and contributors to the EFDA-JET Workprogramme, "Behaviour of disruption generated runaways in jet," *Nuclear Fusion*, vol. 42, no. 8, pp. 1039–1044, 2002.

[8] R. Yoshino, S. Tokuda, and Y. Kawano, "Generation and termination of runaway electrons at major disruptions in jt-60u," *Nuclear Fusion*, vol. 39, no. 2, pp. 151–161, 1999.

[9] T. Fülöp, G. Pokol, P. Helander, and M. Lisak, "Destabilization of magnetosonic-whistler waves by a relativistic runaway beam," *Physics of Plasmas*, vol. 13, no. 6, p. 062506, 2006.

[10] G. Pokol, T. Fülöp, and M. Lisak, "Quasi-linear analysis of whistler waves driven by relativistic runaway beams in tokamaks," *Plasma Physics Controlled Fusion*, vol. 50, 2008.

[11] T. Fülöp, H. Smith, and G. Pokol, "Magnetic field threshold for runaway generation in tokamak disruptions," *Physics of Plasmas*, vol. 16, no. 1, p. 022502, 2009.

[12] P. Helander and D. J. Sigmar, *Collisional Transport in Magnetized Plasmas*. Cambridge University Press, 2002.

[13] R. Jaspers, *Relativistic Runaway Electrons in Tokamak Plasmas*. PhD thesis, Technische Universiteit Eindhoven, 1995.

[14] M. N. Rosenbluth, W. M. MacDonald, and D. L. Judd, "Fokker-planck equation for an inverse-square force," *Phys. Rev.*, vol. 107, pp. 1–6, Jul 1957.

[15] C. F. F. Karney and N. J. Fisch, "Efficiency of current drive by fast waves," *Physics of Fluids*, vol. 28, no. 1, pp. 116–126, 1985.

[16] L.-G. Eriksson and P. Helander, "Simulation of runaway electrons during tokamak disruptions," *Computer Physics Communications*, vol. 154, pp. 175–196, 2003.

[17] H. Dreicer, "Electron and ion runaway in a fully ionized gas. i," *Phys. Rev.*, vol. 115, pp. 238–249, Jul 1959.

[18] H. Dreicer, "Electron and ion runaway in a fully ionized gas. ii," *Phys. Rev.*, vol. 117, pp. 329–342, Jan 1960.

[19] J. Connor and R. Hastie, "Relativistic limitations of runaway electrons," *Nuclear Fusion*, vol. 15, no. 3, pp. 415–424, 1975.

[20] S. Chiu, M. Rosenbluth, R. Harvey, and V. Chan, "Fokker-planck simulations mylb of knock-on electron runaway avalanche and bursts in tokamaks," *Nuclear Fusion*, vol. 38, no. 11, pp. 1711–1721, 1998.

[21] R. W. Harvey, V. S. Chan, S. C. Chiu, T. E. Evans, M. N. Rosenbluth, and D. G. Whyte, "Runaway electron production in diii-d killer pellet experiments, calculated with the cql3d/kprad model," *Physics of Plasmas*, vol. 7, no. 11, pp. 4590–4599, 2000.

[22] H. Smith, P. Helander, L.-G. Eriksson, and T. Fülöp, "Runaway electron generation in a cooling plasma," *Physics of Plasmas*, vol. 12, no. 12, p. 122505, 2005.

[23] H. M. Smith and E. Verwichte, "Hot tail runaway electron generation in tokamak disruptions," *Physics of Plasmas*, vol. 15, no. 7, p. 072502, 2008.

[24] P. B. Parks, M. N. Rosenbluth, and S. V. Putvinski, "Avalanche runaway growth rate from a momentum-space orbit analysis," *Physics of Plasmas*, vol. 6, no. 6, pp. 2523–2528, 1999.

[25] A. B. Rechester and M. N. Rosenbluth, "Electron heat transport in a tokamak with destroyed magnetic surfaces," *Phys. Rev. Lett.*, vol. 40, pp. 38–41, Jan 1978.

[26] P. Helander, L.-G. Eriksson, and F. Andersson, "Suppression of runaway electron avalanches by radial diffusion," *Physics of Plasmas*, vol. 7, no. 10, pp. 4106–4111, 2000.

[27] H. E. Mynick and J. D. Strachan, "Transport of runaway and thermal electrons due to magnetic microturbulence," *Physics of Fluids*, vol. 24, no. 4, pp. 695–702, 1981.

[28] M. Lehnen. Private communication, 2009.

[29] H. Barkhausen, "Zwei mit Hilfe der neuen Verstärker entdeckte Erscheinungen," *Physikalische Zeitschrift*, vol. 20, pp. 401–403, 1919.

[30] T. H. Stix, *Waves in plasmas*. American Institute of Physics, 1992.

[31] D. G. Swanson, *Plasma waves*. Academic Press, 1989.

[32] G. Pokol, *Stability and Statistical Analysis of Transient Waves in Fusion Plasmas*. PhD thesis, Chalmers University of Technology, 2007.

[33] H. Smith, P. Helander, L.-G. Eriksson, D. Anderson, M. Lisak, and F. Andersson, "Runaway electrons and the evolution of the plasma current in tokamak disruptions," *Physics of Plasmas*, vol. 13, no. 10, p. 102502, 2006.

[34] K. Gál, T. Fehér, H. Smith, T. Fülöp, and P. Helander, "Runaway electron generation during plasma shutdown by killer pellet injection," *Plasma Physics Controlled Fusion*, vol. 50, p. 055006, 2008.

[35] V. Plyusnin, V. Riccardo, R. Jaspers, B. Alper, V. Kiptily, J. Mlynar, S. Popovichev, E. de La Luna, F. Andersson, and J. E. contributors, "Study of runaway electron generation during major disruptions in jet," *Nuclear Fusion*, vol. 46, no. 2, pp. 277–284, 2006.

[36] N. Metropolis and S. Ulam, "The monte carlo method," *Journal of the American Statistical Society*, vol. 44, pp. 335–341, September 1949.

[37] M. N. Rosenbluth and S. V. Putvinski, "Theory for avalanche of runaway electrons in tokamaks," *Nuclear Fusion*, vol. 37, no. 10, pp. 1355–1362, 1997.

[38] N. A. Uckan, ed., *Proceedings of the seventh Carolus Magnus Summerschool on plasma and fusion energy physics*, vol. 49 of *Transactions of Fusion Science and Technology*, American Nuclear Society, February 2006.